

GN0: Toward a Unified Paradigm for Generation, Evaluation, and Policy Learning in Visual-Language Navigation

Xinhai Li^{1†‡}, Xiaotao Zhang^{1,2†}, Yuehao Huang^{1,3†}, Jiankun Dong^{1†}, Tianhang Wang^{1,4†}, Sunyao Zhou^{1,5†}, Yunzi Wu^{1,4†}, Chengnuo Sun^{1,6}, Yunfei Ge¹, Qizhen Weng¹, Chi Zhang¹, Chenjia Bai^{1*}, Xuelong Li^{1*}

¹Institute of Artificial Intelligence, China Telecom, ²Shanghai Jiao Tong University, ³Zhejiang University, ⁴Tongji University, ⁵Fudan University, ⁶Jiangsu University

[†]Equal Contributions [‡]Project Leader *Corresponding Authors

Embodied navigation connects intelligent agents with the physical world and serves as a fundamental capability for achieving general robotic intelligence. However, the availability and quality of navigation data have long limited the generalization ability of Vision-and-Language Navigation (VLN) systems and their capacity to handle long-horizon tasks. To bridge this gap, we curate diverse 3D scene resources and develop an automated pipeline for large-scale navigation data generation, resulting in the **GN-Matrix** dataset. Building upon a 3D Gaussian Splatting (3DGS) rendering engine, we further introduce a high-fidelity simulation platform that supports interactive roaming and collision-aware navigation. Furthermore, we propose **GN-Bench**, the first benchmark to provide BEV-based evaluation, incorporating dynamic 3DGS avatars to establish new standards for human-robot interaction evaluation. To fully leverage the interactive nature of the simulator, we develop an RL-driven navigation foundation model, **Break and Establish (BAE)**, after supervised learning, DAgger exposes the model to rollout-induced states and recovery behaviors beyond idealized offline demonstrations, breaking the narrow expert-centric distribution inherited from supervision and providing a better starting point for downstream RL exploration. This unified VLN paradigm seamlessly integrates both map-based and map-free settings, enabling a broad spectrum of tasks including instruction following, human following, and goal navigation. To the best of our knowledge, this work is the first to formalize high-fidelity 3DGS-rendered Bird’s Eye View (BEV) representations as a compact and efficient memory mechanism, thereby unlocking the latent spatial reasoning capabilities of Vision-and-Language Models (VLMs). The dual-system architecture of **GN-BAE** ensures both flexibility and high-efficiency deployment in real-world scenarios. Extensive evaluations on GN-Bench and VLN-CE, encompassing both quantitative and qualitative analyses, demonstrate that the proposed GN0 significantly outperforms existing state-of-the-art VLN methods. Overall, this work, GN-Matrix, presents a unified framework spanning data, simulation, and learning, offering new insights for advancing embodied navigation in both academic research and industrial applications.

Date: June 3, 2026

Project: <https://telehuman-gn0.github.io>.

Code: <https://github.com/TeleHuman/GN0>

Model: <https://huggingface.co/TeleEmbodied/GN-BAE>

Correspondence to: Xinhai Li (lixh92@chinatelecom.cn) Chenjia Bai (baicj@chinatelecom.cn)



1 Introduction

Scene data has always been a critical challenge for Vision-Language Navigation (VLN) [Anderson et al. \(2018a\)](#); [Jain et al. \(2019\)](#); [Krantz et al. \(2020\)](#) large models. The performance of VLN models heavily depends on the quality and fidelity of the scene data they interact with. However, traditional scene representation methods, such as meshes, panoramas, and video sequences, often have limitations in terms of detail rendering

and interactivity. This directly impacts the robustness of VLN performance and leads to a domain gap in applications. 3DGS [Kerbl et al. \(2023\)](#) has recently garnered significant attention in 3D reconstruction, with broad applications in scene reconstruction [Huang et al. \(2024\)](#); [Chen et al. \(2024a\)](#) and 3D asset generation [Poole et al. \(2022\)](#); [Li et al. \(2023\)](#); [Zhao et al. \(2025\)](#); [Xiang et al. \(2025\)](#), and has also inspired growing research in embodied intelligence [Lou et al. \(2025\)](#); [Li et al. \(2024\)](#); [Qureshi et al. \(2025\)](#); [Wang et al. \(2025a\)](#); [Lei et al. \(2025\)](#). Rendering navigation environments with Gaussian Splatting (GS) offers a promising pathway to fully unlock the potential of vision-language models (VLMs). Unlike conventional mesh-based simulators, which often suffer from limited visual fidelity and domain gaps, GS enables photorealistic rendering with rich geometric and appearance details. Meanwhile, approaches that rely on real-world video sequences are constrained by limited coverage, poor controllability, and high data collection costs. Since VLMs are inherently pretrained on large-scale image data, GS provides a more compatible visual interface to transfer pretrained knowledge into embodied navigation. We propose a high-quality 3D scene dataset, GN-Matrix, based on open-source 3DGS scene assets [Miao et al. \(2026\)](#), 3D scene generation [Li et al. \(2025\)](#), self-capture reconstruction scenes [Schönberger et al. \(2016\)](#) and commercially purchased scene assets. This dataset provides strong data support for the development of the field. Additionally, considering that interaction with and service to humans is the ultimate goal of robotics, we have incorporated dynamic 3DGS avatars into the scene, providing high-quality human-robot interaction data to support navigation tasks in dynamic environments [Dong et al. \(2025\)](#). Based on heuristic search and LLM agents, we generated 47 million navigation data sequences in simulated environments, covering tasks such as instruction following, human following, and goal navigation. Each sample includes BEV [Phillion and Fidler \(2020\)](#); [Yang et al. \(2023\)](#) maps, first-person view images, and historical views. The action space consists of both discrete actions and continuous pixel-level trajectories, providing comprehensive data support for training navigation foundation models.

Based on the 3DGS rendering engine, we present an innovative simulation and evaluation platform. This platform supports advanced VLN navigation tasks, including roaming and collision detection, providing models with a more realistic and interactive environment to enhance the navigation experience. A major innovation of this platform is the introduction of dynamic 3DGS avatars benchmark, the first benchmark to provide BEV-based evaluation, offering new evaluation standards for human-robot interaction in VLN. This benchmark effectively evaluates a model’s ability to interact with humans in dynamic, realistic environments, advancing the capabilities of VLN technology.

On the navigation model, we have trained a navigation base model GN-BAE based on GN-Matrix, which is compatible with both map-based [Chen et al. \(2024b\)](#) and map-free [Cai et al. \(2025\)](#) approaches. This flexible design supports various tasks, such as instruction following, human following, and goal navigation. One of the key contributions of this work is the introduction of high-fidelity Bird’s Eye View (BEV) understanding in VLN, making the navigation process more intuitive and efficient. Our Vision-and-Language Model (VLM) [Bai et al. \(2025\)](#) base model is pre-trained on a large number of real images, while the rendered 3DGS images achieve realism comparable to real-world photographs, thereby truly unlocking the potential of VLMs. This innovation not only significantly improves VLN performance but also expands its application across various fields. GN-BAE is trained using reinforcement learning (RL) [?Shao et al. \(2024\)](#) on GN-Bench, activating the spatial perception capabilities of VLMs, enhancing the model’s obstacle avoidance abilities, and effectively addressing data distribution challenges. To promote real-world applications, our model adopts a dual-system architecture, ensuring both flexibility and efficiency. This architecture enables the system to adapt to different application scenarios and environmental requirements, providing support for rapid deployment in both industrial and academic settings.

The seamless integration of GN-Matrix, GN-Bench, GN-BAE provides a comprehensive solution for advancing VLN technology. Our contributions are as follows:

- A high-fidelity scene asset dataset, GN-Matrix, that integrates various indoor and outdoor assets, including open-source, commercial, and generated/reconstructed assets with dynamic 3DGS Avatars, along with a fully automated pipeline for generating navigation task data.
- A fully 3DGS-based navigation simulation platform and benchmark, GN-Bench, which is the first to incorporate BEV evaluation and introduces new evaluation standards for human-robot interaction in dynamic environments with moving agents, while supporting reinforcement learning-based exploration

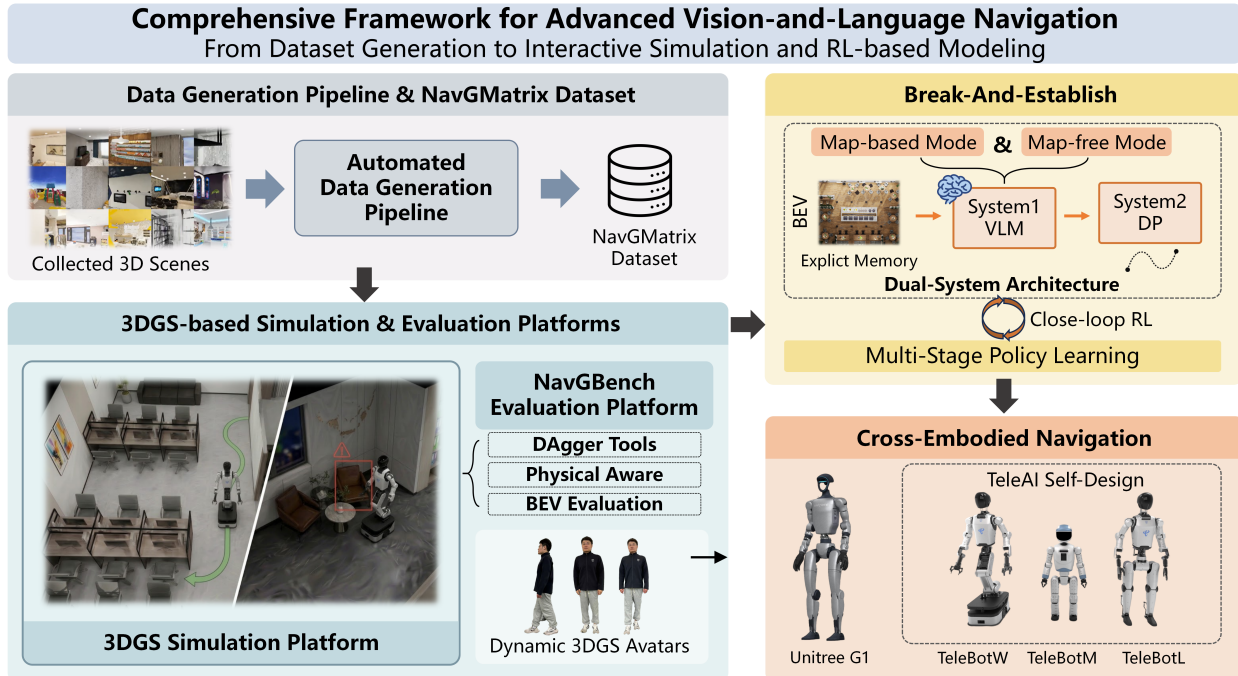


Figure 1 Overview of GN0, including GN-Matrix, GN-Bench, and GN-BAE.

and learning for embodied agents with diverse embodiments within the scene.

- A navigation foundation model, GN-BAE, unifies map-based and map-free paradigms, bridges academic research and industrial deployment. For the first time, high-fidelity 3DGS-rendered BEV representations are formalized as a compact memory mechanism, unlocking the latent spatial reasoning capabilities of VLMs and enabling diverse tasks such as instruction following, human following, and object-goal navigation. The dual-system architecture is optimized for high-throughput industrial inference, while a hybrid “Dagger + RL” training strategy first breaks the narrow expert distribution through DAgger and then enhances corrective exploration and continual learning via reinforcement learning. As a result, GN-BAE achieves state-of-the-art performance on both GN-Bench and VLN-CE benchmarks.

2 Related Works

2.1 Vision-Language Navigation

Embodied Vision-and-Language Navigation (VLN) Wang et al. (2025b); Cao et al. (2025); Gao et al. (2025); Liu et al. (2025); Zhou et al. (2026) studies how agents follow natural-language instructions to move and act in complex environments, which is crucial for enabling embodied intelligence to generate practical value in real-world applications An et al. (2026). Existing methods are commonly developed under either discrete or continuous navigation settings. In discrete VLN Chen et al. (2022a); Zhou et al. (2023), an agent moves over a predefined panoramic connectivity graph. This formulation simplifies high-level reasoning and route selection, but it also removes much of the metric structure, obstacle geometry, and collision constraints that are crucial for embodied deployment Xu et al. (2025). Recent work Zheng et al. (2024); Huang et al. (2025) has further incorporated LLM-based planners and retrieval-augmented memory modules to improve instruction understanding, history utilization, and subgoal decomposition. Nevertheless, these approaches often depend on oracle graph connectivity and provide limited verification of whether the generated plans are physically executable at the low-control level. Continuous VLN aims to close this gap by requiring agents to act directly in metric environments. A common strategy is to combine high-level reasoning with pretrained waypoint prediction, but such predictors can overfit to training environments and may generalize poorly to unseen

layouts or visual conditions. To reduce dependence on scene-specific priors, recent end-to-end dual-system architectures have been explored [Team \(2025\)](#); [Chu et al. \(2026\)](#). These methods typically use a high-level module for embodied reasoning with slow/fast contextual memory, together with a low-level controller, such as a diffusion-policy-based motion module, for responsive local action execution. In this work, we introduce high-fidelity bird’s-eye-view (BEV) representations to construct dual-system memory, providing geometrically grounded spatial context for both long-term reasoning and short-term control, thereby improving navigation robustness in dynamic embodied environments.

2.2 Scene Representations for Vision-Language Navigation

Effective spatial memory plays a central role in enabling embodied VLN agents to perceive, organize, and reason about their surroundings. Existing studies have investigated this problem from different perspectives. ETPNav [An et al. \(2024\)](#) maintains memory through evolvable scene graphs, which support long-horizon navigation by continuously updating topological and semantic relations in the environment. Moving beyond purely topological representations, FOM-Nav [Chabal et al. \(2025\)](#) and 3D-Mem [Yang et al. \(2025\)](#) employ vision-language models (VLMs) to construct and update high-level semantic map memories. By exploiting the zero-shot reasoning ability of VLMs, these methods aim to preserve object-level consistency across observations from different viewpoints. Another line of work investigates implicit memory learning. Uni-NaVid [Zhang et al. \(2025\)](#), for example, adopts an end-to-end video-based architecture to model both short-term and long-term navigation history within latent representations. In contrast to these graph-based, semantic-map-based, or implicit-memory formulations, our method builds an explicit spatial memory using bird’s-eye-view (BEV) representations rendered from 3D Gaussian Splatting [Kerbl et al. \(2023\)](#). This design provides a geometrically grounded memory structure that strengthens both global scene-level spatial awareness and ego-centric local understanding.

2.3 Language-driven Navigation Benchmarks

Recent progress in Vision-and-Language Navigation (VLN) has been closely tied to the development of benchmarks that progressively increase task difficulty, environmental realism, and evaluation fidelity. Early datasets such as Room-to-Room (R2R) [Anderson et al. \(2018a\)](#) and Room-for-Room (R4R) [Jain et al. \(2019\)](#) formulate VLN as instruction following over predefined panoramic paths, where agents are required to execute step-by-step navigation commands in static indoor scenes. Subsequent efforts move beyond discrete panoramic graphs. VLN-CE [Anderson et al. \(2018a\)](#) introduces continuous control in photorealistic simulation environments, placing greater emphasis on visual perception and fine-grained action execution. More recently, VLN-PE [Wang et al. \(2025a\)](#) further improves physical realism by modeling robot dynamics and control imperfections that commonly arise during real-world deployment. Beyond the standard static-environment assumption, several recent benchmarks have begun to explore more complex and interactive navigation settings. HA-VLN [Dong et al. \(2025\)](#) incorporates human activities into VLN scenarios, enabling agents to navigate in environments with dynamic human motion. SocNav [Chen et al. \(2026\)](#) focuses on socially aware navigation by providing diverse social scenes and a comprehensive set of metrics for evaluating human-aware behaviors. In parallel, SAGE-Bench [Miao et al. \(2026\)](#), built upon InteriorGS [SpatialVerse Research Team \(2025\)](#), leverages 3D Gaussian Splatting (3DGS) [Kerbl et al. \(2023\)](#) to transform high-fidelity scene representations from passive perceptual assets into executable environments with semantic and physical alignment for embodied navigation. Other recent benchmarks further expand the scope of VLN toward long-horizon instruction following [Song et al. \(2025\)](#) and collaborative embodied navigation [Wang et al. \(2026\)](#). Beyond standard VLN benchmarks, recent advances in multimodal spatial reasoning provide inspiration for embodied navigation. Models such as AssemLM [Jing et al. \(2026\)](#) demonstrate that integrating point clouds, textual instructions, and visual manuals enables precise 6D pose reasoning and generalization across diverse object categories in robotic assembly tasks. Despite these advances, existing benchmarks still offer limited support for jointly studying 3DGS-based simulation, dynamic agents, and human-robot interaction within a unified navigation framework. To address this gap, we propose GN-Bench, a fully 3DGS-based navigation simulation platform and benchmark designed for human-robot interactive navigation in dynamic environments with moving agents.

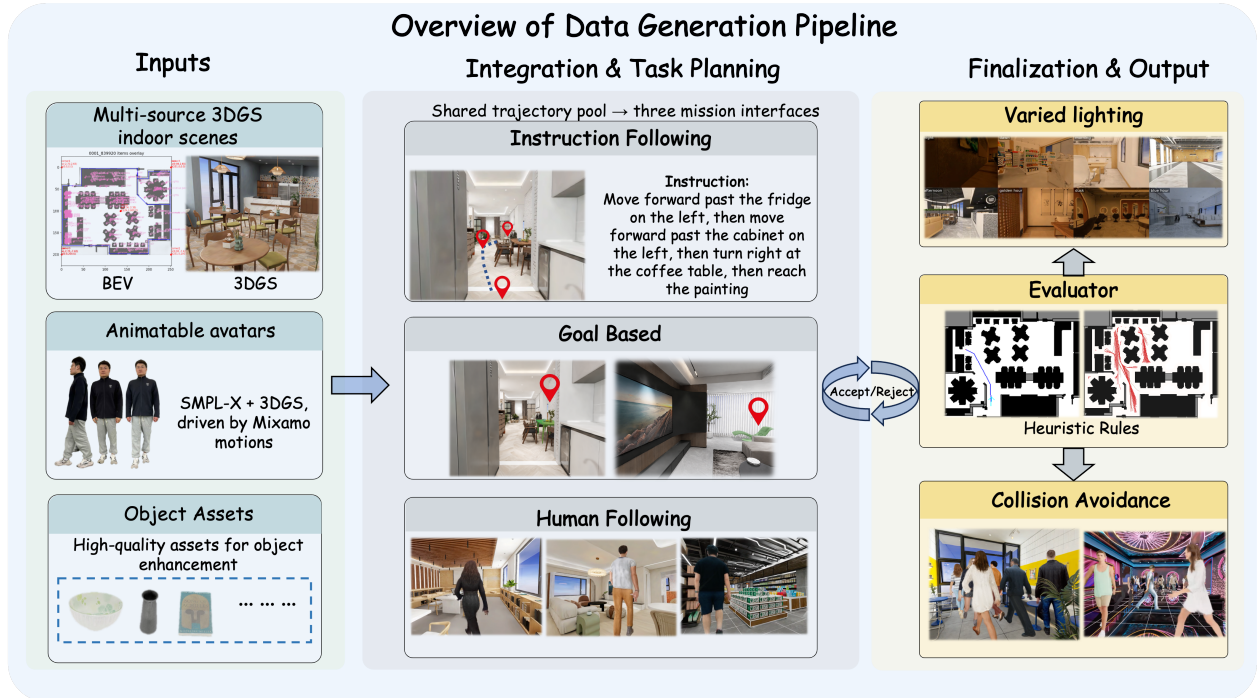


Figure 2 Overview of the GN-Matrix data generation pipeline.

3 Data Generation

3.1 Overview and Key Characteristics

To support large-scale embodied navigation in photorealistic 3D Gaussian Splatting (3DGS) environments, we construct **GN-Matrix**, a large-scale navigation dataset covering diverse indoor scenes, dynamic human-centered environments, and benchmark-compatible data formats for multiple navigation settings [Zhang et al. \(2024\)](#); [Krantz et al. \(2020\)](#); [Wang et al. \(2025a\)](#). To build GN-Matrix, we develop a unified data generation pipeline that integrates multi-source 3DGS scene assets, animated 3DGS human avatars, task synthesis, and multimodal annotation. As illustrated in Fig. 2, this pipeline is designed not only to increase the scale of navigation data, but also to improve scene diversity, task coverage, and realism.

The key characteristics of GN-Matrix are summarized as follows:

- **High-quality 3DGS scene foundation.** GN-Matrix is built on visually faithful 3DGS scene representations, providing realistic observations for embodied navigation in indoor environments.
- **Diverse scene assets.** The dataset combines InteriorGS, handcrafted large-scale scenes, and WorldGrow-expanded scenes to improve scene diversity, layout complexity, and navigational difficulty.
- **Dynamic human avatars.** Beyond static environments, GN-Matrix includes animated 3DGS human avatars with diverse appearances and motions, enabling human-centered embodied navigation settings.
- **Three complementary mission types.** GN-Matrix supports three navigation mission interfaces built on top of a shared trajectory-generation backbone: goal-based navigation, instruction-following navigation, and human-following navigation. These mission types can reuse the same feasible start–goal paths while exposing different forms of task specification, including visual goal references, route-level language specifications, and dynamic human targets.
- **Multimodal and benchmark-compatible supervision.** The dataset provides multimodal annotations and can be adapted to multiple downstream benchmark and training settings, including VLN-CE, VLN-PE, and NaVid.

Within the overall framework of this work, GN-Matrix provides the data foundation, GN-Bench provides the benchmark and simulation environment, and GN-BAE serves as the model baseline.

3.2 Scene Assets

GN-Matrix is built from multiple complementary 3DGS scene sources. Rather than relying on a single dataset, we combine curated indoor reconstructions, handcrafted large-scale scenes, and automatically expanded environments to improve scene diversity, layout complexity, and coverage of navigation difficulty. This multi-source design allows the dataset to provide both high-quality visual grounding and broader coverage of embodied navigation settings.

Unified scene representation. Although these scene sources differ in origin and construction method, they are converted into a unified navigation-ready representation before downstream data generation. This standardization ensures consistent traversability modeling, semantic grounding, rendering interfaces, and coordinate conventions across all scene types, making it possible to apply a shared task synthesis and annotation pipeline throughout the full dataset.

3.2.1 InteriorGS

We take the 1,000 scenes provided by InteriorGS [SpatialVerse Research Team \(2025\)](#) as the main foundation of GN-Matrix. InteriorGS provides realistic indoor 3DGS reconstructions together with semantic annotations, making it a strong starting point in terms of scene quality, visual realism, and object-level grounding. These properties are particularly important for navigation tasks that depend on visually grounded target identification and scene understanding.

At the same time, although InteriorGS provides diverse and well-annotated scenes, its average scene size and layout complexity remain limited for long-horizon embodied navigation. This motivates the inclusion of additional scene sources that emphasize larger-scale spaces and more challenging navigable structures.

3.2.2 Handcrafted Large-Scale Scenes

To complement the InteriorGS base, we introduce 150 handcrafted, dense, large-scale scenes covering environments such as offices and supermarkets. Compared with typical indoor scans, these scenes provide larger navigable areas, more complex spatial layouts, and richer long-range navigation cases.

The main role of this scene source is to expand the dataset toward navigation settings that require longer trajectories, more complex layout reasoning, and denser environmental structure. As a result, the handcrafted scenes strengthen GN-Matrix not only in scale, but also in task difficulty and spatial diversity.

3.2.3 WorldGrow-Expanded Scenes

To further increase scene diversity and overall dataset scale, we also adopt the WorldGrow [Li et al. \(2025\)](#) pipeline to expand the scene set. In contrast to curated and handcrafted scene sources, this component allows us to efficiently generate additional environments and thereby broaden the distribution of indoor layouts, semantics, and navigational conditions represented in the dataset.

Our WorldGrow-based scene expansion follows a structured generation pipeline. First, based on the 3D-FRONT dataset, we develop a scene chunking strategy to extract high-quality and spatially dense scene blocks for training. Second, we improve the structured latent representation in TRELIS [Xiang et al. \(2025\)](#) by introducing an occlusion-aware feature aggregation mechanism and retraining the decoder on scene data, in order to mitigate object occlusion issues and boundary artifacts. Third, we perform 3D block-based inpainting using a flow-matching Transformer, which autoregressively generates adjacent scene blocks conditioned on noise, masks, and known neighboring regions. Through this process, we obtain expanded indoor scenes with improved scale and layout diversity.

The inclusion of WorldGrow-expanded scenes improves the scalability of GN-Matrix and helps reduce over-reliance on a fixed set of manually constructed environments. This is particularly useful for large-scale data generation, where scene diversity is a key factor in improving generalization.

Object quality improvement. To further improve the usability of WorldGrow-expanded scenes, we construct an object enhancement pipeline based on voxel querying and asset replacement. This enables us to replace repetitive, low-quality, or visually corrupted generated objects with higher-quality and more diverse assets derived from HSSD [Khanna* et al. \(2023\)](#). Specifically, we first convert selected HSSD assets into 3D Gaussian representations through a pipeline that renders multi-view images in Blender and then reconstructs Gaussian assets using Gaussian Splatting [Kerbl et al. \(2023\)](#). These assets are then used to replace low-fidelity furniture instances in the generated scenes. This process addresses several shortcomings of WorldGrow-expanded environments, including limited object diversity in color, texture, and structural detail, as well as occasional deformed, warped, or otherwise corrupted objects. As a result, it improves both the visual fidelity and semantic density of the generated scenes, making them more suitable for embodied navigation data generation.

3.3 Dynamic Human Avatars

A key feature that distinguishes GN-Matrix from purely static navigation datasets is the inclusion of dynamic human avatars. Since human-centered interaction is a central objective of embodied intelligence, a navigation dataset should not be limited to empty or static environments. Instead, the agent should operate in scenes that contain diverse human appearances and motions, enabling more realistic evaluation settings such as human-following, dynamic obstacle avoidance, and navigation under time-varying scene conditions.

To construct this component, we build a human avatar bank from single-view human images collected from SHHQ and HuGe100K, supplemented with generated human avatars. For each input image, we recover a parametric SMPL-X body model using SMPLify-X, while separately reconstructing a canonical 3D Gaussian avatar in T-pose using LHM. These two representations provide complementary advantages: the SMPL-X model offers a structured and animatable body prior, while the reconstructed Gaussian avatar preserves the detailed visual appearance of the person.

We then align the SMPL-X mesh to the canonical Gaussian avatar and establish a binding relationship between the body model and the 3DGS representation. This step allows the reconstructed Gaussian avatar to be driven by body motion while preserving its appearance. In our current pipeline, we consider two fitting strategies for this alignment: an ICP-style nearest-neighbor correspondence method and a robust statistical fitting formulation based on Mahalanobis distance. The detailed mathematical formulations are provided in [Appendix A.2](#).

To animate the avatars, we first collect motion assets in FBX format from Mixamo. Each animation sequence is converted into frame-wise SMPL-X parameters, represented as per-frame `smp1x.json` files. These frame-wise body parameters are then used to drive the aligned SMPL-X–Gaussian pair, producing a sequence of animated per-frame Gaussian avatars. This process enables us to combine diverse human appearances with a reusable motion library, thereby constructing dynamic human representations suitable for embodied navigation in human-centered environments.

Overall, the dynamic human avatar component allows GN-Matrix to move beyond static scene navigation and support richer embodied settings in which humans act as moving targets, dynamic scene elements, and future interaction anchors.

3.4 Mission Types and Task Synthesis

GN-Matrix separates trajectory generation from mission presentation. We first construct a shared pool of feasible start–goal trajectories over the traversable regions of each scene, and then instantiate each accepted path under different mission interfaces. This design allows the same spatial path to support multiple forms of supervision: a visual object or region target, a detailed route instruction, or a dynamic human target. As a result, the dataset can evaluate whether navigation agents can follow the same underlying route when the task is specified through different sensory and linguistic interfaces.

For each scene, we begin by collecting candidate target objects and regions from the available semantic scene annotations to form a target pool. Since raw scene annotations may contain multiple nearby instances or repeated targets that do not meaningfully increase navigation diversity, we further filter the target pool to suppress spatially redundant or overlapping endpoints. This ensures that the generated tasks are centered on meaningful navigation goals rather than densely duplicated endpoint choices.

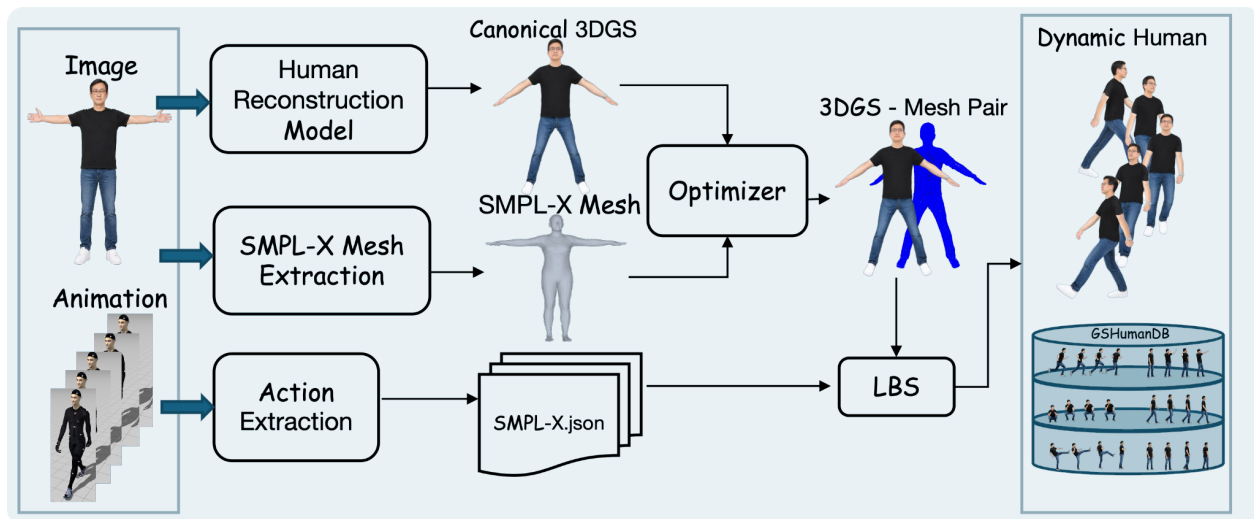


Figure 3 Pipeline for constructing animatable dynamic human avatars, including single-image reconstruction, mesh-Gaussian alignment, and motion-driven avatar generation.

Given the filtered target pool, we sample feasible start-goal pairs over the traversable region of the scene. The goal is not merely to generate as many trajectories as possible, but to construct diverse and non-trivial navigation episodes that cover different spatial regions, path lengths, and scene configurations. To this end, start locations are sampled from valid navigable areas, while goal locations are grounded in semantic targets or selected endpoint regions. For each feasible pair, we then generate a reference navigation trajectory over the scene traversability structure.

To improve dataset quality, we further apply validity and diversity constraints to the generated trajectories. In particular, we remove episodes that are excessively short, spatially trivial, or highly similar to previously accepted paths. This filtering step encourages the final dataset to cover broader navigation patterns and reduces the over-representation of near-duplicate trajectories. Each accepted trajectory is then packaged with reference path information, waypoint or action supervision, and the metadata required to instantiate the three mission types described below.

3.4.1 Goal-Based Navigation Tasks

We first instantiate each accepted trajectory as a goal-based navigation task. In this setting, the mission specifies the destination through a rendered goal reference or target observation, together with a concise target-oriented instruction. The agent is required to ground the target within the 3DGS scene and navigate to the corresponding endpoint.

Unlike instruction-following navigation, this mission type specifies the destination without explicitly prescribing the intermediate route. Each episode is packaged with the goal reference, target semantics, start pose, reference trajectory, and downstream waypoint or action supervision. These generated tasks can later be converted into multimodal training instances with first-person observations, bird’s-eye-view context, action or waypoint supervision, and benchmark-compatible formats.

3.4.2 Instruction-Following Navigation Tasks

The second mission type is instruction-following navigation. In this setting, the underlying start-goal path can be identical to the goal-based trajectory, but the task specification is provided as a route-level natural-language instruction. Rather than specifying only the destination, the instruction describes intermediate navigation constraints, including landmark references, relative directions, and ordered spatial decisions along the path.

This setting corresponds to the route-following interface used in many vision-language navigation benchmarks. The instruction provides intermediate constraints along the path, requiring the agent to align language with

local observations, maintain progress over a long-horizon route, and execute the navigation sequence in the correct order.

To generate these tasks, we convert each accepted reference trajectory into a route-level language specification using the scene semantics, landmark visibility, turning points, and endpoint context along the path. The resulting episode shares the same spatial trajectory as the corresponding goal-based task, but exposes a different input interface. This decoupling allows GN-Matrix to compare goal-based navigation and language-guided route following under matched path geometry and scene difficulty.

Each instruction-following episode is packaged with the route instruction, start pose, endpoint metadata, reference trajectory, and downstream supervision signals. These tasks support instruction-conditioned training and evaluation while preserving the same 3DGS grounding and action-space conventions used by the rest of the dataset.

3.4.3 Human-Following Tasks

Beyond traditional static goal-based navigation and instruction-following navigation, GN-Matrix also supports human-following tasks in which the agent is required to follow a moving human target through the scene. Compared with the other two types of navigation, the target in this setting is no longer a fixed semantic endpoint, but a dynamic human whose position evolves over time. This task family therefore provides a more realistic testbed for human-centered embodied navigation in dynamic environments.

To construct these tasks, we instantiate animated human avatars inside the scene and assign them motion trajectories derived from the dynamic avatar pipeline described in Section 3.3. Rather than generating an entirely independent trajectory source, we adapt trajectories from the shared trajectory pool and reinterpret them as human motion paths. In this way, the dynamic human target inherits feasible and scene-consistent navigation behavior while extending the dataset from static semantic goals to moving human-centered targets.

Given a moving human trajectory, we then construct a corresponding agent-follow episode in which the agent navigates relative to the target motion rather than toward a fixed endpoint. In particular, the task is designed to preserve a reasonable following relationship, such as maintaining a preferred relative distance and viewpoint with respect to the moving target, while still adapting to scene geometry and time-varying occlusion. This transforms the shared reference trajectory into a dynamic navigation problem with continuous target tracking.

Compared with static goal-based and instruction-following navigation, human-following introduces additional challenges including motion-aware path adjustment, changing target visibility, and the need to remain robust to dynamic scene configurations. These properties make it a useful benchmark setting for evaluating embodied navigation systems in more realistic human-centered environments.

Each generated human-following episode is packaged with the target human identity, the underlying motion trajectory, the associated agent trajectory, and downstream supervision signals. These tasks can therefore support multimodal training and evaluation for dynamic navigation, while also serving as a foundation for future extensions toward richer human-agent interaction scenarios.

3.5 Benchmark Compatibility and Dataset Statistics

In addition to serving as a native 3DGS-based embodied navigation dataset, GN-Matrix is also designed to support compatibility with existing embodied navigation benchmarks and training settings. Rather than treating these benchmarks as separate data sources, we view them as target export formats built on top of the same scene-grounded task generation pipeline. This design allows GN-Matrix to preserve its original spatial and semantic grounding while remaining usable within established embodied navigation ecosystems.

To improve interoperability with existing benchmarks, we adapt the generated mission specifications into benchmark-compatible formats. Depending on the target setting, goal-based, instruction-following, and human-following missions can be reformulated into benchmark-compatible interfaces aligned with VLN-CE, VLN-PE, and NaVid, while preserving the underlying scene-grounded trajectory and navigation semantics.

Beyond instruction adaptation, we also convert the generated reference trajectories into benchmark-compatible discrete action sequences. This step is important because many embodied navigation benchmarks and policy

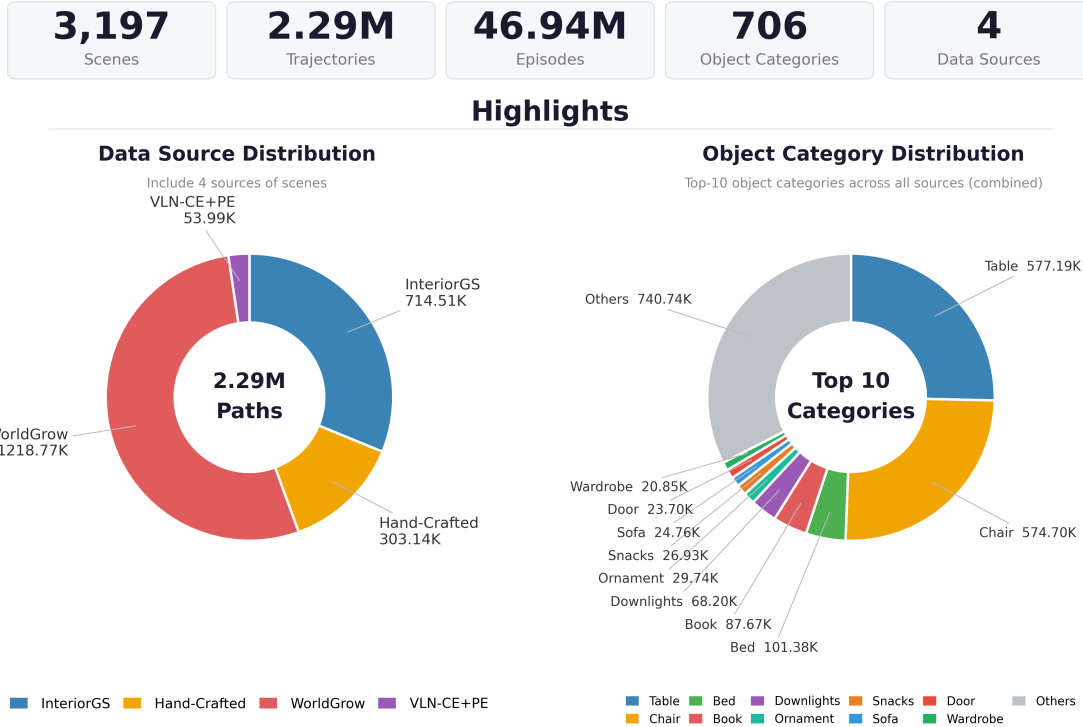


Figure 4 Dataset statistics of GN-Matrix. We summarize the overall dataset scale and composition of the generated navigation data, including the number of scenes, trajectories, episodes, object categories, data sources, source distribution, and object-category distribution.

learning frameworks operate on discrete control spaces rather than continuous trajectory representations. By aligning the generated task data with this control convention, GN-Matrix can be used more directly for downstream training and evaluation in standard navigation setups.

Using the above pipeline, we construct a large-scale navigation dataset covering both static and dynamic embodied navigation tasks. GN-Matrix contains multi-source indoor scenes, dynamic human-centered episodes, and diverse mission types including goal-based navigation, instruction-following navigation, and human-following navigation. We further rebalance the raw action distribution to reduce the dominance of forward actions and improve the usefulness of the dataset for policy learning. The final dataset scale, mission composition, and train/validation/test split are summarized in the main paper, while detailed conversion rules and benchmark-specific export settings are provided in the appendix.

Table 1 Summary of benchmark compatibility and dataset outputs.

Setting	Instruction Format	Action Space	Notes
Native GN-Matrix	Goal / instruction / human-following mission formats	Path / action supervision	3DGS-based representation
VLN-CE / VLN-PE / NaVid	Adapted	Discrete	Benchmark-compatible export

3.6 DAgger Data Collection

To mitigate compounding errors caused by the covariate shift between offline expert demonstrations and online policy execution, we construct an exploratory dataset utilizing the Dataset Aggregation (DAgger) algorithm. During this collection phase, the agent actively explores the environments driven by the initial

SFT policy. At each visited state s_t , the system dynamically relabels the current observation with optimal expert annotations for both continuous waypoints and discrete actions.

For goal-based and instruction-following missions, the oracle planner uses the static endpoint as the destination. For human-following missions, the oracle instead tracks the time-indexed human trajectory and generates corrective labels relative to the desired following state.

For the continuous pixel trajectory, we query the integrated oracle planner. By executing the A* search algorithm [Hart et al. \(1968\)](#) over the dilated occupancy grid \mathcal{M}_{dil} , we extract the optimal, collision-free geodesic path from the current planning state to the destination g . This global path is subsequently projected into the agent’s egocentric frame to formulate the ground-truth BEV waypoint sequence $\mathcal{T}_{bev,t}^*$.

Concurrently, to generate the discrete action labels, we formulate a Model Predictive Control (MPC) strategy [Richalet et al. \(1978\)](#). The MPC optimizes a short-horizon control sequence to track the A* reference path, yielding the optimal VLN-CE compliant macro-action $a_t^* \in \{\langle \text{FWD} \rangle, \langle \text{LEFT} \rangle, \langle \text{RIGHT} \rangle, \langle \text{STOP} \rangle\}$. This expert action selection is formalized as minimizing the tracking cost over a predictive horizon H :

$$a_t^* = \arg \min_{a \in \mathcal{A}} \sum_{k=1}^H \gamma^k \mathcal{C}(s_{t+k}, \mathcal{T}_{bev,t}^*) \quad (1)$$

where γ is a discount factor and \mathcal{C} denotes the spatial deviation cost from the optimal A* trajectory.

Furthermore, to prevent the agent from infinitely hovering near the target without asserting task completion, we enforce a strict halting heuristic. Let $d(p_t, g)$ denote the spatial distance between the agent’s current coordinate p_t and the goal g , and let $d_{success}$ define the task success radius. Upon entering the success region ($d(p_t, g) \leq d_{success}$), the system initializes a localized step counter c_{goal} . If the agent executes 10 additional steps without emitting the termination token, the simulation environment forcibly truncates the episode. Under this condition, the expert label for the terminal state is explicitly overwritten to supervise the halting behavior:

$$a_t^* = \langle \text{STOP} \rangle, \quad \text{if } d(p_t, g) \leq d_{success} \text{ and } c_{goal} \geq 10 \quad (2)$$

This aggregated dataset of on-policy states coupled with oracle-corrected targets provides the necessary corrective supervision to expand the policy space, directly supporting the entropy increase phase prior to GRPO training.

3.7 Post-processing and Dataset Balancing

After task synthesis, we further improve the quality and usability of GN-Matrix through post-processing and data balancing. These steps are designed to increase both visual diversity and learning utility in the final dataset.

Visual-condition enhancement. To improve robustness to appearance variation, we construct an enhancement pipeline that generates additional data under diverse lighting conditions by manipulating illumination intensity and color schemes. This process produces visually varied observations while preserving the underlying navigation semantics of each task, thereby broadening the visual coverage of the final dataset.

Action distribution balancing. The raw generated trajectories are strongly biased toward forward actions, with comparatively fewer turning and stopping actions. To reduce this imbalance, we rebalance the final dataset by adjusting the relative proportions of forward, turning, and stop actions. This improves the usefulness of the dataset for downstream navigation policy learning and reduces the tendency of models to over-predict straight motion.

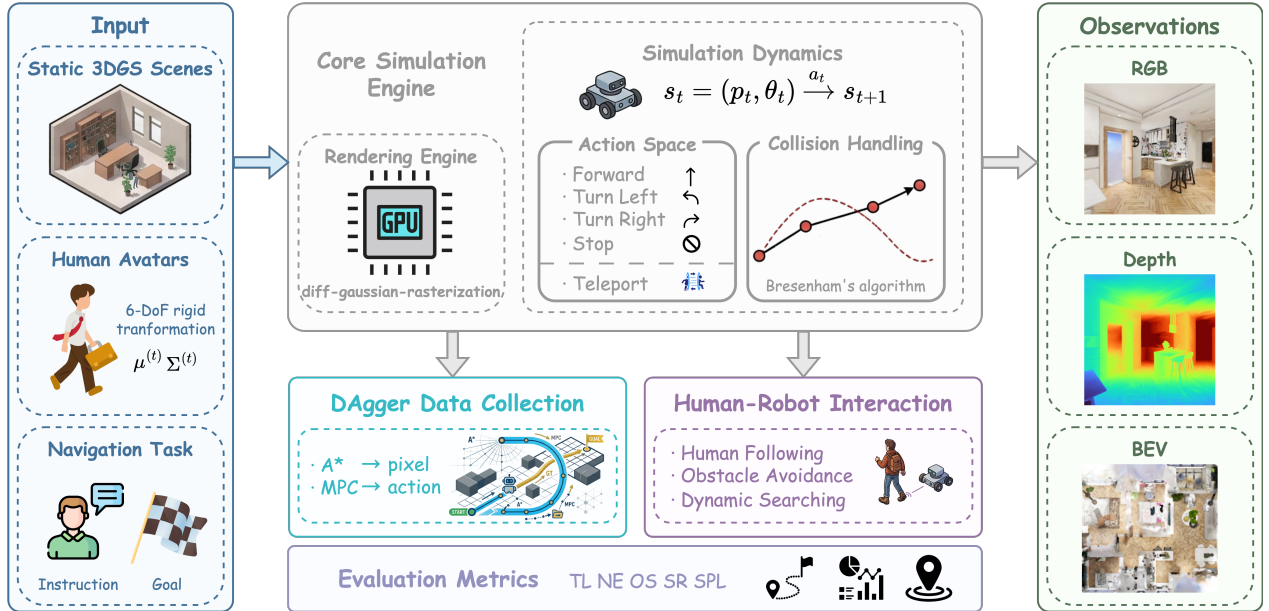


Figure 5 Overview of GN-Bench and its high-fidelity interactive simulation capabilities.

4 GN-Bench

GN-Bench is a high-fidelity embodied navigation benchmark built on 3D Gaussian Splatting indoor environments, designed to provide a unified platform for both policy evaluation and data generation under realistic closed-loop interaction. Beyond photorealistic egocentric RGB observations, GN-Bench supports metric-consistent BEV rendering, enabling a unified benchmark for both map-free and map-conditioned navigation paradigms. The simulator integrates rendering, motion execution, collision handling, and geodesic planning into a single interactive loop, allowing agents to be evaluated under physically constrained online execution rather than static offline replay. Importantly, GN-Bench also provides oracle planning and online relabeling capabilities, which make it possible to construct DAgger-style corrective supervision directly from policy rollouts. This allows the benchmark to serve not only as an evaluation substrate, but also as a practical training environment for studying recovery behaviors, covariate-shift mitigation, and closed-loop policy improvement in embodied navigation.

4.1 Core Rendering Engine

GN-Bench leverages the highly optimized `diff-gaussian-rasterization` framework Kerbl et al. (2023) as its core rendering engine. Designed to meet the high-throughput requirements of embodied AI research, this backend employs an efficient 3DGS pipeline to concurrently generate high-resolution RGB images and spatially aligned depth maps. Furthermore, this streamlined architecture facilitates cross-scene generalization, allowing standardized agent and sensor configurations to be seamlessly deployed across diverse environments through the direct instantiation of pre-trained Gaussian assets.

4.2 Simulation Dynamics and Interactivity

GN-Bench inherits and expands upon the robust simulation mechanics established by industry-standard platforms such as Habitat Savva et al. (2019) and NavGSim Liu et al. (2026). The platform is equipped with a comprehensive suite of embodied AI features:

4.2.1 Observation Space

To support diverse embodied navigation paradigms, GN-Bench provides a comprehensive, multi-modal observation space, summarized in Table 2. The simulator concurrently renders high-resolution egocentric

RGB-D streams via perspective cameras and high-fidelity Bird’s Eye View (BEV) projections. The BEV representations are synthesized by configuring a virtual downward-facing camera with an orthogonal projection matrix within the 3DGS rendering pipeline. This orthographic rasterization explicitly preserves metric scale by bypassing perspective foreshortening, thereby supplying a geometrically consistent spatial prior essential for global map-based planning.

Table 2 The multi-modal observation space generated by GN-Bench. The simulator supports the simultaneous rendering of egocentric and top-down perspectives to facilitate both map-free and map-based navigation paradigms. Image resolution ($H \times W$) and Field of View (FoV) are fully configurable hyperparameters.

Modality	Camera Type	Tensor Shape	FoV / Scale	Primary Downstream Utility
Egocentric RGB	Perspective	$H \times W \times 3$	Configurable	Visual semantic reasoning for VLMs
Egocentric Depth	Perspective	$H \times W \times 1$	Configurable	Local geometry & reactive obstacle avoidance
Top-down BEV	Orthographic	$H_{bev} \times W_{bev} \times C$	Metric-scale	Global spatial prior & topological planning

4.2.2 Action Space and Kinematics

To accommodate varying levels of navigational autonomy, the simulator defines the agent’s spatial state at time step t as $s_t = (p_t, \theta_t)$, where $p_t \in \mathbb{R}^2$ is the 2D coordinate and $\theta_t \in [-\pi, \pi)$ is the heading angle. The platform supports a hybrid action space $\mathcal{A} = \mathcal{A}_{local} \cup \mathcal{A}_{global}$. For fine-grained exploration, agents execute VLN-CE compliant discrete actions $a \in \mathcal{A}_{local}$ with fixed translation step Δd and rotation angle $\Delta\theta$. The kinematic update function is formalized as:

$$s_{t+1} = \begin{cases} (p_t + \Delta d \cdot [\cos \theta_t, \sin \theta_t]^\top, \theta_t), & \text{if } a = \text{MoveForward} \\ (p_t, \theta_t \pm \Delta\theta), & \text{if } a = \text{TurnLeft/Right} \end{cases} \quad (3)$$

Alternatively, to evaluate accelerated high-level waypoint planning, the system accepts global actions $a \in \mathcal{A}_{global}$. This enables direct spatial teleportation to explicitly defined global coordinates p_{target} , yielding an instantaneous state update $s_{t+1} = (p_{target}, \theta_{target})$. This dual formulation seamlessly bridges low-level continuous control with topological routing strategies.

4.2.3 Collision Handling

To enforce rigorous physical constraints, GN-Bench implements a deterministic collision detection module based on the intrinsic grayscale occupancy maps from the GN-Matrix dataset. Let \mathcal{M} denote the binary occupancy grid where obstacles are defined as 1. To mathematically account for the agent’s physical footprint of radius r , we apply a morphological dilation using a circular structuring element \mathcal{B}_r . This yields the expanded obstacle map $\mathcal{M}_{dil} = \mathcal{M} \oplus \mathcal{B}_r$, which effectively transforms the collision boundaries relative to the agent’s center of mass. For any proposed kinematic translation from a source coordinate p_{src} to a target p_{dst} , the trajectory is discretized into a finite sequence of grid pixels via Bresenham’s line algorithm [Bresenham \(1965\)](#). This sequence, denoted as $\mathcal{P} = (p_0, p_1, \dots, p_N)$ with $p_0 = p_{src}$ and $p_N = p_{dst}$, is sequentially evaluated against \mathcal{M}_{dil} . If the path intersects an occupied cell, the movement vector is strictly truncated. The agent’s spatial state is then updated to the final collision-free coordinate $p_{final} = p_k$ along the intended trajectory, formalized as:

$$k = \max\{i \in [0, N] \mid \mathcal{M}_{dil}(p_j) = 0, \forall j \leq i\} \quad (4)$$

As expressed in Eq. 4, this discrete formulation ensures penetration-free continuous roaming while maintaining high computational efficiency during large-scale simulation.

4.2.4 Global Path Planning

GN-Bench incorporates an oracle path planner to facilitate goal-oriented navigation and standardized benchmarking. The system applies the A* heuristic search algorithm [Hart et al. \(1968\)](#) directly to the dilated occupancy grids. Because these grids explicitly account for the agent’s physical footprint, the planner reliably computes optimal, collision-free trajectories between any traversable states. This deterministic formulation yields the ground-truth geodesic distances required to evaluate core metrics such as Success

weighted by Path Length (SPL) [Anderson et al. \(2018b\)](#). Concurrently, it acts as an expert demonstrator to synthesize the oracle annotations required for our DAGger data collection pipeline (as described in Sec. 3.6), thereby providing direct supervision for the training of map-based navigation policies.

4.3 Dynamic 3DGS Avatars and Human-Robot Interaction

A critical limitation of conventional VLN simulators is their reliance on strictly static environments. To address this, GN-Bench seamlessly integrates dynamic 3DGS human avatars into the foundational GN-Matrix scenes, thereby synthesizing highly realistic, non-stationary navigation scenarios.

From a rendering perspective, let \mathcal{G}_{static} denote the set of 3D Gaussians representing the static indoor environment, and \mathcal{G}_{avatar} denote the Gaussians of the human avatar. At each simulation time step t , the avatar is driven by a spatiotemporal trajectory specifying its 6-DoF pose, defined by a rotation matrix R_t and a translation vector T_t . To dynamically render the human within the scene, we apply a rigid transformation to the mean μ_i and covariance Σ_i of each Gaussian $i \in \mathcal{G}_{avatar}$:

$$\mu_i^{(t)} = R_t \mu_i + T_t, \quad \Sigma_i^{(t)} = R_t \Sigma_i R_t^\top \quad (5)$$

The updated avatar Gaussians $\mathcal{G}_{avatar}^{(t)}$ are then concatenated with \mathcal{G}_{static} before the unified rasterization pass. By introducing these spatiotemporally varying human subjects, our platform establishes a novel paradigm for evaluating dynamic Human-Robot Interaction (HRI). This formulation inherently supports the rigorous benchmarking of complex, time-critical embodied tasks, specifically active target following and reactive dynamic obstacle avoidance. Consequently, GN-Bench extends standard VLN evaluation protocols to better reflect the unpredictability of real-world robotic deployment in populated spaces.

5 GN-BAE

Break and Establish (BAE) is a unified embodied navigation foundation model for instruction following, human following, and goal-directed navigation, following the general formulation of vision-and-language navigation and continuous embodied navigation [Anderson et al. \(2018a\)](#); [Krantz et al. \(2020\)](#). It supports FPV, BEV, and hybrid visual inputs, while jointly modeling both discrete action sequences and continuous trajectories within a single framework. At its core, BAE adopts a trajectory tokenization scheme that unifies planning representation and improves training efficiency across diverse navigation settings. Combined with high-fidelity rendered data [Kerbl et al. \(2023\)](#) and supervised fine-tuning, this design effectively unlocks the navigation capability of the underlying vision-language model. A key component is our closed-loop post-training pipeline: after supervised learning, DAGger [Ross et al. \(2011\)](#) exposes the model to rollout-induced states and recovery behaviors beyond idealized offline demonstrations, breaking the narrow expert-centric distribution inherited from supervision and providing a better starting point for downstream exploration. Building on this initialization, DAPO [Yu et al. \(2025\)](#) further refines the policy with execution-oriented rewards, enabling more effective exploration, stronger long-horizon decision-making, and more reliable action generation during rollout. Lightweight Action Experts further bridge high-level planning and executable control for practical deployment [Cai et al. \(2025\)](#).

The model architecture is composed of five components. During Vision-and-Language Navigation (VLN) training [Anderson et al. \(2018a\)](#); [Krantz et al. \(2020\)](#), coordinate tokenization significantly enhances efficiency, simplifies the learning process, and unifies task execution. By leveraging GS high-fidelity rendering [Kerbl et al. \(2023\)](#) with Supervised Fine-Tuning (SFT), we can activate the latent pre-trained knowledge of Qwen3-VL [Bai et al. \(2025\)](#), preserving as much of the pre-training knowledge as possible. In the reinforcement learning process, increasing entropy helps expand the exploration range of the policy, thereby improving the diversity and scope of learning. Furthermore, on the RL-trained Vision-and-Language Model (VLM), we employ Action Expert [Cai et al. \(2025\)](#) to adapt to different ontologies, enabling cross-ontology capability transfer while significantly improving edge inference efficiency. The combination of these techniques results in a more efficient training process, providing enhanced adaptability and superior inference performance in real-world applications.

The tasks include a variety of capabilities, such as instruction following, human following, and goal navigation. The system is designed to handle different types of visual input, including Bird’s Eye View (BEV), First-Person

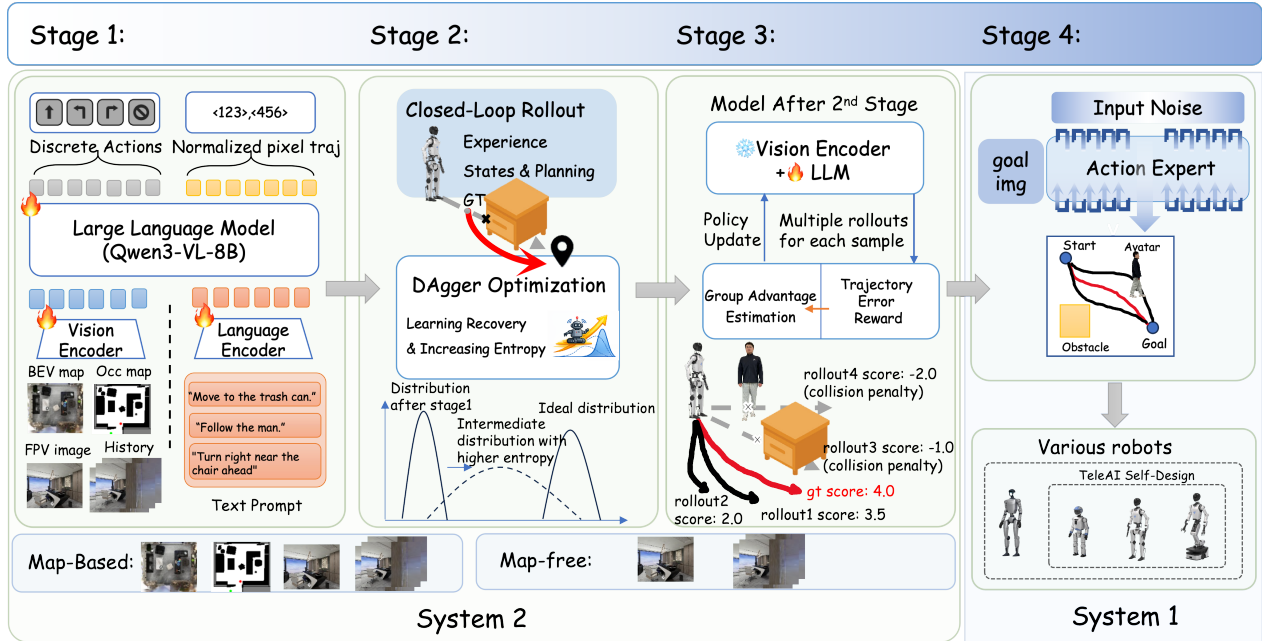


Figure 6 Architecture of BAE and its Four-Stage Training Strategy of DAGger + RL.

View (FPV), or a combination of both BEV and FPV. Additionally, the output trajectories can be represented in two formats: discrete actions, which correspond to specific movement commands, or continuous trajectory points, which provide a denser representation of the planned path. This flexibility in both input modalities and output formats enables the model to support a broad range of navigation scenarios under a unified framework.

For FPV-based navigation, we introduce a simple memory mechanism to compensate for the lack of global spatial context. Specifically, the current frame observation is treated as short-term memory, while the observations associated with the previous sixteen executed discrete actions are used as long-term memory. These sixteen historical observations are concatenated into a single image and fed into the model together with the current frame. As a result, the FPV input contains not only the current egocentric view, but also a compact visual history aligned with the recent action sequence, which improves temporal reasoning and action prediction.

5.1 Trajectory tokenization

We formulate trajectory prediction as discrete sequence generation instead of direct continuous regression. For autoregressive VLMs, discrete token prediction is generally easier to optimize, more stable across heterogeneous tasks, and more convenient for unifying different output ontologies. Inspired by sequence-based visual prediction and location-token modeling [Chen et al. \(2022b,c\)](#); [Peng et al. \(2024\)](#); [Jiang et al. \(2025\)](#), we adopt a tokenized trajectory representation for both discrete actions and continuous waypoints. In particular, following the idea of relative coordinates with special tokens, we map continuous spatial outputs into a bounded discrete token space, which reduces learning difficulty and improves token efficiency.

For trajectories represented by discrete actions, we define a lightweight action vocabulary consisting of `<action>`, `</action>`, `<FWD>`, `<LEFT>`, `<RIGHT>`, and `<STOP>`. Here, `<action>` and `</action>` indicate the action span, while the four atomic action tokens follow the VLN-CE action semantics [Krantz et al. \(2020\)](#): `<FWD>` moves the agent forward by 0.25 meters, `<LEFT>` rotates the agent left by 15 degrees, `<RIGHT>` rotates the agent right by 15 degrees, and `<STOP>` terminates navigation. This design converts low-level control decisions into a compact symbolic sequence and allows the model to learn action policies through standard next-token prediction.

For trajectories represented by continuous points, we discretize normalized BEV coordinates into 1,000 bins

and assign one special token to each bin, i.e., $\langle 0 \rangle$ to $\langle 999 \rangle$. Each waypoint is first projected onto the BEV plane and then normalized with respect to the current BEV canvas size, so that all coordinates are represented in a shared token space. This is particularly useful in our setting because BEV images may have different resolutions across datasets and tasks. Without normalization, the same physical location could correspond to different pixel values, which increases the learning burden. By contrast, relative coordinates with special tokens provide a unified and resolution-agnostic representation, while also requiring fewer output tokens than coordinate strings or digit-level serialization.

With this design, BAE supports both action-sequence prediction and waypoint-sequence prediction under the same autoregressive modeling framework, providing a common representation layer across different navigation tasks and deployment ontologies.

5.2 VLM SFT

During the SFT stage, we train BAE with standard supervised fine-tuning on trajectory-token prediction. Given a multimodal input x and a target trajectory token sequence y^* , the training objective is the autoregressive cross-entropy loss:

$$\mathcal{L}_{\text{SFT}}(\theta) = -\mathbb{E}_{(x, y^*) \sim \mathcal{D}} \left[\frac{1}{L} \sum_{t=1}^L \log \pi_{\theta}(y_t^* | y_{<t}^*, x) \right]. \quad (6)$$

The supervision targets are constructed from both discrete actions and pixel-space trajectories. Specifically, we use the next six discrete actions as the action label sequence, and a future 3-meter trajectory in the BEV space as the continuous trajectory label. The 3-meter trajectory is uniformly discretized into 12 pixel points, which are then converted into trajectory tokens using the tokenization scheme described above. For pure FPV input, we do not apply the pixel-trajectory output branch, and the training target only contains the discrete action sequence.

We jointly finetune the entire model, including the vision encoder, the multimodal projector, and the language model. To stabilize training, we use a smaller learning rate for the vision tower (2×10^{-6}), while setting the learning rates of the multimodal projector and the LLM to 1×10^{-5} . This imitation learning stage establishes the basic planning capability of the VLM for downstream navigation tasks.

5.3 DAgger-based Closed-loop Adaptation

A policy obtained from pure supervised fine-tuning is often overly concentrated around idealized expert trajectories, which may be suboptimal for subsequent reinforcement learning. In our setting, this issue is further exacerbated because the SFT targets are derived from ideal A* trajectories [Hart et al. \(1968\)](#). While such supervision is effective for learning canonical navigation behaviors, it provides limited coverage of recovery actions under closed-loop execution, where the agent may deviate from the intended path and must correct errors induced by its own previous decisions. As a result, a model initialized solely from SFT may have limited support over the state-action distribution encountered at the beginning of GRPO training [Shao et al. \(2024\)](#).

To mitigate this mismatch, we introduce an additional DAgger stage before GRPO [Ross et al. \(2011\)](#); [Shao et al. \(2024\)](#):

$$\mathcal{L}_{\text{DAgger}}(\theta) = -\mathbb{E}_{(x, y^*) \sim \mathcal{D}_{\text{DAgger}}} \left[\frac{1}{L} \sum_{t=1}^L \log \pi_{\theta}(y_t^* | y_{<t}^*, x) \right]. \quad (7)$$

In practice, we collect 284k closed-loop DAgger samples and optimize the model for 5 epochs with a learning rate of 1×10^{-6} . During this stage, we continue updating the full VLM, including the vision encoder, rather than freezing the visual backbone. Importantly, this stage is not intended to drive the training loss to a very low level. Instead, its purpose is to adapt the post-SFT policy toward the state distribution induced by real closed-loop rollouts, where trajectory deviations and corrective behaviors naturally arise.

This design serves two closely related goals. First, DAgger improves the model’s ability to recover from realistic closed-loop perturbations, which is beneficial to navigation performance in its own right. More importantly, it provides a better initialization for GRPO. From a distributional perspective, DAgger moves

the policy away from the overly concentrated SFT solution toward an intermediate distribution that better balances ideal expert behavior and the empirical state distribution encountered during closed-loop execution. Such an initialization increases the likelihood of sampling reasonable trajectories in the early stage of DAPO, and thereby facilitates more effective exploration and optimization in subsequent reinforcement learning.

5.4 DAPO

After the DAgger stage, we further optimize BAE with DAPO under closed-loop interaction [Yu et al. \(2025\)](#). Although DAgger already improves the policy’s robustness to the state distribution induced by its own actions, it remains fundamentally an imitation-style training stage [Ross et al. \(2011\)](#). To further improve long-horizon decision quality and directly optimize execution-oriented objectives, we introduce a reinforcement learning stage built upon the DAgger-initialized model.

Before DAPO training, we first use the post-DAgger model to interact with the environment in a closed-loop manner, following a data collection procedure similar to that used in the DAgger stage. In this way, we collect an additional 22k closed-loop samples. These samples are not used as supervised labels; instead, they serve as the reference basis for reward computation during DAPO training. Compared with directly starting reinforcement learning from the pure SFT model, this design produces an initial rollout distribution that is substantially closer to realistic execution trajectories, thereby improving reward reliability and stabilizing the early stage of policy optimization.

For policy optimization, we adopt the GRPO-style advantage estimator [Shao et al. \(2024\)](#) within the DAPO framework [Yu et al. \(2025\)](#). Given an input x , the current policy π_θ samples a group of G candidate responses $\{y_1, y_2, \dots, y_G\}$, where each response corresponds to a complete predicted trajectory. For each sampled response y_i , we compute a scalar reward r_i based on the execution-oriented reward defined below. The reward is then normalized within the group to obtain a relative advantage,

$$A_i = \frac{r_i - \text{mean}(r_1, \dots, r_G)}{\text{std}(r_1, \dots, r_G)}. \quad (8)$$

In this way, policy optimization is driven by relative trajectory quality within each sampled group, so that trajectories with better rollout outcomes receive larger positive updates, while worse trajectories are suppressed.

Following the DAPO/GRPO formulation [Shao et al. \(2024\)](#); [Yu et al. \(2025\)](#), we optimize the policy with a clipped policy-gradient objective [Schulman et al. \(2017\)](#):

$$\mathcal{J}_{\text{DAPO}}(\theta) = \frac{1}{G} \sum_{i=1}^G \frac{1}{|y_i|} \sum_{t=1}^{|y_i|} \min(\rho_{i,t} A_i, \text{clip}(\rho_{i,t}, 1 - \epsilon_{\text{low}}, 1 + \epsilon_{\text{high}}) A_i), \quad (9)$$

where

$$\rho_{i,t} = \frac{\pi_\theta(y_{i,t} \mid x, y_{i,<t})}{\pi_{\theta_{\text{old}}}(y_{i,t} \mid x, y_{i,<t})} \quad (10)$$

is the importance ratio between the updated and behavior policy at token step t . This objective preserves the core idea of policy-gradient optimization while preventing excessively large updates through ratio clipping.

The necessity of DAPO in our setting can be understood from two aspects. First, under standard SFT, trajectory generation is optimized only through teacher-forced next-token prediction. Such supervision is effective for learning the required format and canonical expert behavior, but it does not distinguish whether a sampled trajectory is globally better at the rollout level. By contrast, DAPO allows gradient updates to be weighted by trajectory-level quality, rather than treating all target tokens equally under next-token prediction. Second, this design is especially important for our normalized pixel branch. Although normalized coordinate tokens provide an efficient representation for waypoint prediction, they also introduce a mismatch between discrete token supervision and continuous geometric quality. Two predictions that differ by only one coordinate token may correspond to a negligible spatial deviation, while predictions with similar token-level losses may lead to substantially different rollout quality. Therefore, for the normalized pixel branch, reinforcement learning is necessary to bridge this discrete-to-continuous gap by directly optimizing geometry-aware trajectory similarity, rather than relying solely on token-level supervision.

In our implementation, each prompt samples 8 candidate responses during rollout. We disable KL regularization in both the actor loss and the reward term, and optimize the model with a learning rate of 1×10^{-6} . This choice is made empirically: we observe that enabling KL loss can easily destabilize optimization in tasks with strong output-format constraints, and in severe cases may even cause the policy to collapse with respect to the required action-generation format. In our setting, such regularization is unnecessary, since format validity is already explicitly enforced by the reward design, which assigns large penalties to invalid predictions and therefore serves as an effective safeguard for structured generation. During this stage, we freeze the vision tower and update only the remaining trainable components of the VLM. After SFT and DAgger, the visual backbone is already sufficiently adapted to the rendered navigation observations, while the primary role of reinforcement learning is to further refine action generation behavior rather than relearn visual perception.

The reward function is designed as an execution-oriented structured score. Given a predicted action sequence \hat{a} and its reference action sequence a^* , we define the overall reward as

$$R(\hat{a}, a^*) = R_{\text{traj}} + \lambda_{\text{first}} R_{\text{first}} - \lambda_{\text{col}} R_{\text{col}} - \lambda_{\text{len}} R_{\text{len}} - \lambda_{\text{fmt}} R_{\text{fmt}}, \quad (11)$$

where R_{traj} measures rollout-level consistency between the predicted and reference trajectories under shared initial conditions, R_{first} rewards correct prediction of the first action, R_{col} penalizes collision during rollout, R_{len} penalizes length mismatch between the predicted and reference action sequences, and R_{fmt} denotes the format penalty for invalid structured outputs. The trajectory term jointly considers both positional consistency and heading consistency under closed-loop rollout. Overall, this reward encourages the model to generate responses that are not only structurally valid, but also dynamically consistent with the reference behavior and executable in the environment.

In practice, the DAPO stage is trained with a batch size of 64, while 8 responses are sampled for each prompt during rollout. We optimize the model for 2 epochs.

Moreover, our ablation study further shows that directly applying DAPO without the DAgger stage does not lead to meaningful performance improvement. A plausible reason is that, after Stage 1, the policy entropy is already very low, which severely limits exploration at the beginning of reinforcement learning and consequently prevents DAPO from yielding substantial capability gains.

5.5 Action Expert

For waypoint-based outputs, we do not directly execute the predicted pixel trajectory. Instead, we first transform the predicted BEV trajectory into the agent-centered first-person world coordinate frame, and then feed it into a dedicated NavDP Action Expert [Cai et al. \(2025\)](#) to generate executable low-level actions. We train the Action Expert from scratch following the training pipeline and loss design of the InternNav repository. In practice, we maintain two separate experts for different task families, namely a follow expert and a planning expert. The Action Expert is introduced not only to produce smoother and more stable action execution, but also to improve safety in cluttered environments by providing stronger local obstacle avoidance capability. In this way, the VLM is responsible for high-level trajectory planning, while the Action Expert serves as a trajectory-to-action adapter that improves execution robustness and safety.

To better align the Action Expert with the VLM input modality, we remove the depth input from the original NavDP design [Cai et al. \(2025\)](#) and use only visual observations and goal-related conditions. NavDP is trained with a DDPM-style noise prediction objective [Ho et al. \(2020\)](#), following diffusion-policy-based visuomotor learning [Chi et al. \(2023\)](#); [Cai et al. \(2025\)](#), where Gaussian noise is added to the target action trajectory and the model learns to predict the injected noise:

$$\mathbf{a}_\tau = \sqrt{\bar{\alpha}_\tau} \mathbf{a} + \sqrt{1 - \bar{\alpha}_\tau} \boldsymbol{\epsilon}, \quad \boldsymbol{\epsilon} \sim \mathcal{N}(\mathbf{0}, \mathbf{I}), \quad (12)$$

$$\mathcal{L}_{\text{act}} = \mathbb{E} \left[\|\hat{\boldsymbol{\epsilon}}_\theta(\mathbf{a}_\tau, \tau, \cdot) - \boldsymbol{\epsilon}\|_2^2 \right]. \quad (13)$$

In addition to the diffusion action loss, the training objective also includes a critic regression term for obstacle-aware trajectory quality estimation and an auxiliary cross-modal goal alignment term [Cai et al. \(2025\)](#). The overall loss is

$$\mathcal{L} = 0.8 \mathcal{L}_{\text{act}} + 0.2 \mathcal{L}_{\text{critic}} + 0.5 \mathcal{L}_{\text{aux}}. \quad (14)$$

6 Experiments

6.1 Experiment Setup

Simulated environments. We conduct evaluations across three distinct simulation platforms. **GN-Bench** serves as our primary high-fidelity, 3DGS-based continuous navigation environment. **VLN-CE** provides a standard benchmark built upon the Habitat simulator [Savva et al. \(2019\)](#) and Matterport3D scenes, focusing on natural language instruction following under continuous control. Finally, **VLN-PE** offers a physics-aware framework that accurately models the real-world dynamics and low-level control errors of a Unitree H1 humanoid robot, bridging the sim-to-real gap.

Real-world environments. To evaluate the model’s performance in real-world environments, we conducted three experiments across multiple robotic platforms, including a self-developed wheeled–arm robot TeleBotW, a self-developed small humanoid robot TeleBotM, and the Unitree Robotics G1 humanoid robot. The system was deployed on an NVIDIA Orin edge device, while inference was executed on an NVIDIA H100 GPU, achieving a real-time inference frequency of up to 5 Hz.

Metrics. To comprehensively evaluate navigation performance in continuous and physically realistic environments, we adopt standard metrics for both task completion and kinematic stability. Specifically, we measure Navigation Error (NE), defined as the terminal Euclidean distance to the goal; Success Rate (SR), the percentage of episodes where the agent halts within a 3-meter success radius; and Oracle Success (OS), indicating whether any point along the agent’s trajectory breaches the success threshold. To quantify path efficiency, we report Trajectory Length (TL) as the total physical distance traversed, alongside Success weighted by Path Length (SPL), which heavily penalizes detours.

Baselines. We compare GN-BAE against a diverse spectrum of state-of-the-art visual navigation methods. These encompass traditional multi-sensor paradigms reliant on panoramic RGB, depth, and odometry (e.g., CMA, ETPNav), VLM-free single-view RGB-D approaches, and recent Video-LLM architectures restricted solely to egocentric RGB inputs (e.g., NaVid, InternNav).

6.2 Simulated Environment

6.2.1 Evaluation on GN-Bench

We first evaluate GN-BAE on the GN-Bench benchmark (Table 3). While traditional methods rely on auxiliary depth, recent VLM-based baselines and our approach operate strictly on monocular RGB (FPV) or Bird’s Eye View (BEV). Despite this minimal sensory constraint, GN-BAE establishes a new state-of-the-art by a massive margin. Notably, on the Unseen split, our FPV-only variant achieves a 38.9% SR, outperforming the

Table 3 Evaluation Metrics on GN-Bench. In the observation space, **Depth** denotes depth maps, **BEV** refers to Bird’s Eye View projections, and **FPV** represents first-person RGB images. **Bold** represents the best results. Underline indicates the second best results. [†] Indicates methods fine-tuned via SFT on the NavGMatrix dataset.

Method	Observation			Metrics on Seen					Metrics on Unseen				
	Depth	BEV	FPV	TL	NE ↓	OS ↑	SR ↑	SPL ↑	TL	NE ↓	OS ↑	SR ↑	SPL ↑
CMA	✓		✓	2.9	8.3	15.7	12.5	11.9	3.0	8.1	19.6	15.5	14.9
NaVid			✓	3.4	7.9	20.1	14.6	12.8	3.5	7.7	20.3	14.5	12.8
UniNaVid			✓	4.6	7.9	22.2	15.0	12.5	5.2	7.8	20.7	12.8	10.3
InternNav(S2)			✓	3.6	7.4	23.1	18.8	17.5	3.7	7.2	26.7	22.1	20.3
NaVid [†]			✓	2.7	7.4	19.4	18.8	18.8	2.7	7.1	23.8	23.1	23.0
UniNaVid [†]			✓	3.7	7.2	24.1	22.5	21.9	5.8	7.5	23.1	20.8	20.2
InternNav(S2) [†]			✓	2.9	7.1	22.5	22.4	22.4	2.9	6.9	24.9	24.0	23.7
GN-BAE			✓	5.2	<u>4.9</u>	<u>48.9</u>	<u>46.4</u>	<u>44.7</u>	5.0	5.6	43.6	38.9	<u>37.3</u>
GN-BAE		✓	✓	5.2	4.3	59.3	58.6	58.6	4.0	<u>5.8</u>	<u>40.2</u>	<u>38.5</u>	38.2

Table 4 Comparison with state-of-the-art methods on VLN-CE R2R Val-Unseen split. * indicates methods using the waypoint predictor from Hong et al. (2022).

Method	Observation				R2R Val-Unseen			
	Pano.	Odo.	Depth	S.RGB	NE ↓	OS ↑	SR ↑	SPL ↑
HPN+DN*	✓	✓	✓		6.31	40.0	36.0	34.0
CMA*	✓	✓	✓		6.20	52.0	41.0	36.0
GridMM*	✓	✓	✓		5.11	61.0	49.0	41.0
ETPNav*	✓	✓	✓		4.71	65.0	57.0	49.0
ScaleVLN*	✓	✓	✓		4.80	-	55.0	51.0
InstructNav	✓	✓	✓	✓	6.89	-	31.0	24.0
R2R-CMTP	✓	✓	✓		7.90	38.0	26.4	22.7
LAW		✓	✓	✓	6.83	44.0	35.0	31.0
CM2		✓	✓	✓	7.02	41.5	34.3	27.6
WS-MGMap		✓	✓	✓	6.28	47.6	38.9	34.3
ETPNav + FF		✓	✓	✓	5.95	55.8	44.9	30.4
Seq2Seq			✓	✓	7.77	37.0	25.0	22.0
CMA			✓	✓	7.37	40.0	32.0	30.0
NaVid				✓	5.47	49.1	37.4	35.9
MapNav				✓	4.93	53.0	39.7	37.2
NaVILA				✓	5.22	62.5	54.0	49.0
UniNaVid				✓	5.58	53.3	47.0	42.7
StreamVLN				✓	4.98	64.2	56.9	51.9
DualVLN				✓	4.05	70.7	64.3	58.5
CorrectNav				✓	4.24	67.5	65.1	62.3
GN-BAE				✓	3.50	75.6	67.7	63.4

strongest fine-tuned baseline InternNav-S2[†] by nearly 15 absolute points, demonstrating exceptional spatial reasoning in a low-level action space.

Comparing our two variants reveals an insightful trade-off between modality and generalization. On the Seen split, the BEV-augmented model dominates, indicating that global geometric priors substantially facilitate navigation in familiar environments. However, on the Unseen split, the FPV-only variant yields better NE, OS, and SR, while the BEV variant only retains a marginal edge in SPL. This suggests that while BEV improves path efficiency, imperfect map cues in novel 3DGS environments can introduce representation bias, occasionally misleading long-horizon decisions. Conversely, the FPV-only policy relies on robust egocentric visual-language grounding, proving to be more resilient to scene-level distribution shifts for goal reaching.

6.2.2 Evaluation on VLN-CE

We evaluate GN-BAE on the standard R2R-CE benchmark using the Validation Unseen split. As shown in Table 4, GN-BAE achieves the best overall performance, reaching 3.50 NE, 75.6 OS, 67.7 SR, and 63.4 SPL using only single-view RGB input. Compared with the strongest prior RGB-only baseline, GN-BAE reduces NE by 17.5%(from 4.24 to 3.50m) while improving SR and SPL by 2.6 and 1.1 points, respectively, indicating better goal localization and trajectory efficiency.

We attribute this improvement to the proposed offline reinforcement learning paradigm. Unlike conventional SFT-based navigation models, which mainly learn to imitate token-level action labels, GN-BAE further



Figure 7 Experiment in Real-world Environment with self-developed wheeled-arm robot TeleBotW and Unitree Robotics G1 humanoid robot.

optimizes the policy distribution toward high-quality navigation trajectories. In particular, the DAgger-style stage exposes the model to states induced by its own policy, mitigating covariate shift caused by long-horizon closed-loop execution. The subsequent offline RL stage then encourages actions that are more consistent with successful and efficient navigation behavior, rather than merely matching the marginal action distribution of the training data. As a result, the learned policy better aligns with the ideal navigation distribution, leading to stronger generalization in unseen environments.

6.3 Experiment in Real-world Environment

Trained solely on high-fidelity Gaussian Splatting (GS) simulation data, our model demonstrates strong sim-to-real generalization capability. Notably, the model is able to accomplish real-world tasks reliably without any exposure to real robot data during training.

As illustrated in the figure 7, the three experimental tasks are defined as follows:

The robot moves straight into a circular dark room, exits through the door on the right-hand side, and continues forward until reaching the vicinity of a table. Starting near the table, the robot proceeds forward while following the curtain on its left-hand side, turns right at the corner, and continues straight until reaching a glass door. Starting from the glass door, the robot turns right and moves along the corridor, enters the first door on the left, passes a water dispenser, continues straight to the end of the hallway, turns right, and finally stops near a round table in the corridor.

6.4 Ablation Studies

To systematically evaluate the efficacy of the proposed three-stage training pipeline, we conduct comprehensive ablation experiments on both seen and unseen environments, with results summarized in Table 5. This analysis isolates the empirical contributions of each distinct learning phase to the overall navigation performance.

Effectiveness of DAgger Adaptation. The baseline model, trained exclusively via SFT on the GN-Matrix dataset, establishes foundational instruction-following capabilities but suffers from severe policy degradation due to compounding errors in out-of-distribution states. Incorporating the intermediate DAgger stage effectively mitigates this covariate shift. By exposing the agent to rollout-induced states and injecting corrective oracle supervision, this phase relaxes policy over-concentration and expands search entropy. Consequently, we observe a substantial boost in both SR and OS, demonstrating enhanced state coverage and online execution stability.

Benefits of Preference-Driven RL. Building upon the robust initialization provided by DAgger, the terminal DAPO stage further aligns the policy with long-horizon execution objectives. As manifested in Table 5, ablating this reinforcement learning phase (“w/o DAPO”) leads to a noticeable drop in efficiency. The full pipeline consistently minimizes NE and maximizes SPL across both FPV and BEV-conditioned settings. This confirms that while imitation learning stages anchor basic navigation semantics, the preference-driven RL phase is critical for refining sequential decision-making and optimizing global trajectory efficiency.

Table 5 Ablation study of the proposed training pipeline on the validation split. The “w/o” prefix signifies the ablation of a specific stage from the complete pipeline.

Method	Observation		Metrics on Seen					Metrics on Unseen				
	BEV	FPV	TL	NE ↓	OS ↑	SR ↑	SPL ↑	TL	NE ↓	OS ↑	SR ↑	SPL ↑
Full Pipeline		✓	5.3	4.9	49.5	46.9	45.1	5.0	5.6	43.6	38.9	37.3
w/o DAgger		✓	3.0	6.7	27.5	26.5	25.8	4.9	5.7	42.4	37.8	36.0
w/o DAPO		✓	5.0	5.2	45.4	41.9	40.2	3.1	6.8	29.9	28.1	27.3
w/o DAgger & DAPO		✓	4.1	6.5	28.9	26.1	24.8	4.1	6.4	32.9	29.4	28.1
Full Pipeline	✓	✓	5.2	4.3	59.4	58.7	58.6	4.0	5.8	40.2	38.5	38.2
w/o DAgger	✓	✓	3.0	6.9	26.9	25.6	25.0	3.2	6.4	33.5	32.4	32.3
w/o DAPO	✓	✓	4.2	5.4	48.0	47.6	47.4	3.1	6.8	30.4	27.8	26.9
w/o DAgger & DAPO	✓	✓	3.8	6.8	27.2	23.6	22.4	4.0	6.6	31.4	27.6	26.4

7 Discussion

This work presents, to the best of our knowledge, the first unified embodied navigation framework spanning data, simulation, model, and evaluation. By constructing the largest high-fidelity 3DGS-based navigation dataset to date and developing an interactive 3DGS simulator, GN-Matrix provides a scalable foundation for long-horizon embodied navigation.

We further introduce GN-Bench, a new benchmark for evaluating embodied navigation with BEV-based metrics and dynamic 3DGS avatars, enabling more realistic assessment of spatial reasoning and human-robot interaction. Built on this framework, BAE combines supervised learning, DAgger, and reinforcement learning to improve robustness under rollout-induced distribution shifts, while 3DGS-rendered BEV serves as an efficient spatial memory for unified map-based and map-free navigation.

Extensive experiments show that GN-BAE achieves state-of-the-art performance on both VLN-CE and GN-Bench. Beyond simulation, it transfers effectively to real robots and supports cross-embodiment adaptation across humanoid and wheeled platforms, highlighting its practical potential for general embodied intelligence.

Despite these advances, incorporating richer physical interactions and extending the framework toward more complex embodied tasks remain important future directions.

A Additional Details of Data Generation

This appendix provides additional technical details for the data generation process of NavGMatrix, including scene-source breakdown, dynamic human avatar construction, task synthesis details, benchmark compatibility adaptation, and expanded dataset statistics.

A.1 Detailed Scene Source Breakdown and Category Taxonomy

In this section, we provide a more detailed breakdown of the scene assets used to construct NavGMatrix. In particular, we summarize the contributions of InteriorGS, handcrafted large-scale scenes, and WorldGrow-expanded scenes to the overall dataset.

We further categorize scenes by environment type and report additional statistics such as scene counts, layout complexity, room count, and representative examples. These statistics complement the high-level scene description in the main paper and help illustrate the scale and diversity of the underlying 3DGS scene corpus.

A.1.1 WorldGrow Scene Generation Prompts

To expand the scene distribution beyond curated indoor scans, we use text-conditioned scene generation for WorldGrow-expanded environments. An example prompt used for generating a high-detail residential scene is

Table 6 Detailed scene-source breakdown for GN-Matrix.

Source	# Scenes	Main Categories	Avg. Scene Size (m ²)	Avg. Object Count	Notes
InteriorGS	1,000	Indoor residential	150.1	502.9	High-quality indoor 3DGS scenes with semantic annotations
Handcrafted large-scale scenes	150	Large-scale commercial (office/supermarket)	374.5	2321.4	Dense large-scale environments such as offices and supermarkets
WorldGrow-expanded scenes	1760 / 240	6x6 and 8x8 indoor scenes	91.68 / 158.76	N/A	Automatically expanded scenes for improving diversity and scale

shown below:

A photorealistic 3D residence mesh with a Victorian Vintage style, featuring ornate wood paneling and velvet-upholstered seating areas that lavishly incorporate tufted sofas, carved armchairs, roll-top desks, four-poster beds, and display cabinets with intricate woodwork. Use crystal chandeliers and stained glass lamps to create rich, layered lighting. Prioritize detailed topology for decorative surfaces and hand-carved wooden components for opulence, maintaining a luxurious and ornate historical aesthetic.

These prompts are designed to control both global scene style and local object richness, thereby improving the diversity, density, and visual fidelity of automatically expanded environments.

A.2 Dynamic Human Avatar Construction Details

Single-image avatar reconstruction. For each input human image, we recover a parametric SMPL-X body model using SMPLify-X and reconstruct a canonical 3D Gaussian avatar in T-pose using LHM. This produces two complementary representations: a structured body prior and a visually faithful Gaussian avatar.

Mesh-Gaussian alignment and binding. We align the SMPL-X mesh to the canonical Gaussian avatar and construct an aligned SMPL-X-Gaussian pair that allows avatar appearance to be driven by body motion. We consider two fitting strategies: (1) nearest-neighbor pairing with ICP-style refinement, and (2) a robust statistical fitting formulation based on Mahalanobis distance.

Animation retargeting and motion driving. We collect motion assets in FBX format from Mixamo and convert them into frame-wise SMPL-X parameters. These per-frame parameters are then used to drive the aligned SMPL-X-Gaussian pair and produce animated per-frame Gaussian avatar sequences.

Avatar and motion statistics. We additionally summarize the scale and diversity of the dynamic human avatar component, including the number of reconstructed identities, appearance keyword coverage, motion categories, and animation counts.

A.2.1 Problem setup

Let the SMPL-X body model be parameterized by shape β and pose θ , with vertices and joints denoted by $V(\beta, \theta) = \{v_i\}_{i=1}^{N_V}$ and $J(\beta, \theta) = \{j_m\}_{i=1}^{N_J}$, respectively. After applying a global alignment transform, the transformed source points are denoted by

$$\tilde{v}_i = R_{\text{pre}}(Rv_i + t), \quad \tilde{j}_m = R_{\text{pre}}(Rj_m + t),$$

where $R \in SO(3)$ is the current global rotation, $t \in \mathbb{R}^3$ is the global translation, and $R_{\text{pre}} \in SO(3)$ is an optional fixed pre-rotation.

Let the canonical Gaussian avatar be represented by a set of Gaussian components

$$\mathcal{G} = \{(\mu_k, \Sigma_k, \alpha_k)\}_{k=1}^{N_G},$$

where $\mu_k \in \mathbb{R}^3$ is the Gaussian center, $\Sigma_k \in \mathbb{R}^{3 \times 3}$ is the covariance matrix, and $\alpha_k \in [0, 1]$ is the opacity or confidence weight. We write the corresponding precision matrix as

$$\Lambda_k = \Sigma_k^{-1}.$$

A.2.2 ICP-style nearest-neighbor fitting

Given a transformed source point x , we first retrieve a candidate neighbor set $\mathcal{N}(x)$ from the Gaussian centers using Euclidean distance. A soft correspondence centroid is then defined as

$$q(x) = \sum_{k \in \mathcal{N}(x)} w_k(x) \mu_k, \quad w_k(x) = \frac{\alpha_k \exp\left(-\frac{\|x - \mu_k\|_2^2}{\sigma_d^2}\right)}{\sum_{\ell \in \mathcal{N}(x)} \alpha_\ell \exp\left(-\frac{\|x - \mu_\ell\|_2^2}{\sigma_d^2}\right)}.$$

Using the resulting source–target pairs $(x, q(x))$, we form a trimmed rigid alignment objective

$$\mathcal{L}_{\text{rigid}} = \frac{1}{|\mathcal{S}_{\text{trim}}|} \sum_{x \in \mathcal{S}_{\text{trim}}} \omega(x) \rho(\|x - q(x)\|_2),$$

where $\mathcal{S}_{\text{trim}}$ denotes the retained source set after trimming large-residual correspondences, $\omega(x)$ is a scalar correspondence confidence, and $\rho(\cdot)$ is a robust loss such as the Huber loss.

A.2.3 Robust Mahalanobis fitting

To better account for anisotropic Gaussian geometry, we also consider a hard Mahalanobis assignment objective. For each source point x , we choose the best-matching Gaussian index

$$k^*(x) = \arg \min_{k \in \mathcal{N}(x)} (x - \mu_k)^\top \Lambda_k (x - \mu_k).$$

The corresponding robust fitting loss is

$$\mathcal{L}_{\text{maha}} = \frac{1}{|\mathcal{S}_{\text{trim}}|} \sum_{x \in \mathcal{S}_{\text{trim}}} \rho\left(\sqrt{(x - \mu_{k^*(x)})^\top \Lambda_{k^*(x)} (x - \mu_{k^*(x)})}\right).$$

A.2.4 Optional soft-assignment refinement

As an alternative soft correspondence formulation, we may define a Gaussian mixture assignment around each source point. The soft weight of Gaussian k for source point x is

$$\pi_k(x) = \frac{\alpha_k \exp\left(-\frac{1}{T} (x - \mu_k)^\top \Lambda_k (x - \mu_k)\right)}{\sum_{\ell \in \mathcal{N}(x)} \alpha_\ell \exp\left(-\frac{1}{T} (x - \mu_\ell)^\top \Lambda_\ell (x - \mu_\ell)\right)},$$

where T is a temperature parameter. The corresponding soft Mahalanobis loss can be written as

$$\mathcal{L}_{\text{soft}} = \frac{1}{|\mathcal{S}|} \sum_{x \in \mathcal{S}} \sum_{k \in \mathcal{N}(x)} \pi_k(x) \rho\left(\sqrt{(x - \mu_k)^\top \Lambda_k (x - \mu_k)}\right).$$

A.2.5 Anchor and regularization terms

To stabilize alignment, we may additionally use anchor constraints on selected joints:

$$\mathcal{L}_{\text{anchor}} = \frac{1}{|\mathcal{A}|} \sum_{m \in \mathcal{A}} \text{Huber}(\|\tilde{j}_m - a_m\|_2; \delta),$$

where \mathcal{A} is an anchor joint set and a_m is the target anchor position for joint m .

A regularized pose refinement objective can then be written as

$$\mathcal{L}_{\text{fit}} = \lambda_{\text{rigid}} \mathcal{L}_{\text{rigid}} + \lambda_{\text{maha}} \mathcal{L}_{\text{maha}} + \lambda_{\text{soft}} \mathcal{L}_{\text{soft}} + \lambda_{\text{anchor}} \mathcal{L}_{\text{anchor}} + \lambda_{\text{prior}} \mathcal{L}_{\text{prior}},$$

where $\mathcal{L}_{\text{prior}}$ denotes body pose and shape regularization.

A.2.6 Avatar animation pipeline

Given the aligned SMPL-X–Gaussian pair, we convert motion sequences from Mixamo FBX assets into frame-wise SMPL-X parameters $\{\theta_t\}_{t=1}^T$. For each frame t , the corresponding body parameters are applied to the aligned SMPL-X model, and the resulting motion is transferred to the Gaussian avatar through the learned binding relationship. This yields an animated per-frame Gaussian avatar sequence

$$\{\mathcal{G}_t\}_{t=1}^T.$$

Table 7 Suggested appendix table for avatar and motion statistics.

Category	Used Count	Notes
Human identities		Reconstructed avatar count
- SHHQ identities	76	Source breakdown
- HuGe100K identities	100	Source breakdown
Motion categories	4	Walking / Running / Waving / Idle

A.3 Detailed Task Generation Algorithms

A.3.1 Goal-Based Navigation Task Generation

Task formulation and target construction. For each scene, we first construct a candidate target pool from the available semantic scene annotations. Each candidate target corresponds to a meaningful object instance or target region that can serve as a navigation goal. Since raw annotations may contain nearby duplicated instances, heavily overlapping targets, or semantically redundant endpoints, we further apply redundancy suppression to obtain a cleaner goal set for task generation.

The purpose of this step is to ensure that the resulting goal-based navigation tasks are grounded in semantically meaningful scene targets rather than arbitrary endpoints. This improves the interpretability of the generated tasks and strengthens compatibility with downstream instruction generation and benchmark conversion.

Implementation-aligned target construction. We do not merge object instances via IoU at the target construction stage. Instead, near-duplicate endpoints are suppressed later through path-level similarity filtering, which better preserves semantic target coverage while removing redundant episodes.

Start-goal sampling and reference path generation. After constructing the filtered target pool, we sample feasible start-goal pairs over the traversable region of the scene. Start positions are sampled from valid navigable space, while goal positions are grounded in semantic targets. For each feasible pair, we generate a reference trajectory over the scene traversability representation to obtain a navigation path from the sampled start state to the target.

To avoid excessive concentration around a small number of spatial regions, the sampling process is designed to encourage broader spatial coverage across the scene. This improves task diversity and produces a wider range of path lengths and spatial configurations.

Planning and diversification algorithm. For each cleaned semantic target, we generate a reference trajectory on the inflated safe occupancy grid. The target location is fixed to its snapped safe-grid goal, and the start is sampled from the same connected component to guarantee reachability. To improve spatial coverage, the sampler uses inverse-density zone weighting when scene-level visitation statistics are available, otherwise biases sampling toward locations far from previously used points, and falls back to uniform component sampling when no coverage prior is provided.

The sampled start and target goal are connected with A* search on the safe grid using local grid connectivity and obstacle-aware traversal. Invalid searches are discarded. Valid trajectories are then simplified by line-of-sight smoothing, densified with rasterized line segments, and adaptively resampled into compact keypoints.

Algorithm 1 Goal Target Construction and Safe Goal Snapping

Require: Occupancy map, occupancy metadata, structure annotations, semantic labels

Ensure: Filtered semantic target set \mathcal{T}

```
1: Load grayscale occupancy image and optional wall mask
2: Compute traversable grid by thresholding occupancy values
3: Inflate obstacles with safety margin to obtain safe grid  $\mathcal{G}_{\text{safe}}$ 
4: Load wall segments from scene structure annotations
5: Compute connected components on  $\mathcal{G}_{\text{safe}}$ 
6:  $\mathcal{T} \leftarrow \emptyset$ 
7: for each semantic instance  $e$  in labels.json do
8:   Compute object centroid  $(c_x, c_y, c_z)$  from its bounding box
9:   Convert centroid to pixel location  $g_{\text{raw}}$ 
10:   $g \leftarrow \text{FINDNEARESTSAFE}(g_{\text{raw}}, \mathcal{G}_{\text{safe}}, \text{walls})$ 
11:  if  $g$  is invalid then continue
12:  end if
13:  if  $g$  does not belong to any valid connected component then continue
14:  end if
15:  Add target record
      {ins_id, label, centroid_world, goal_pixel, goal_component}
16:  to  $\mathcal{T}$ 
17: end for
18: return  $\mathcal{T}$ 
```

Finally, all geometric annotations are converted from pixel space to world space, and the initial facing direction is estimated from the first trajectory segment, yielding a target-grounded navigation record with start, goal, keypoints, dense trajectory, and metadata.

Trajectory validity and diversity filtering. Not all generated reference trajectories are retained in the final dataset. To improve overall data quality, we apply a series of validity and diversity filters to remove undesirable episodes. In particular, we reject trajectories that are too short, spatially trivial, highly similar to previously accepted paths, or insufficiently distinct in their start–goal configuration.

These filters reduce the number of near-duplicate or low-information episodes and help the final dataset better represent long-horizon, diverse navigation behavior. As a result, the accepted task set is more balanced in both path geometry and spatial coverage.

Post-generation filtering algorithm. After generation, candidate trajectories are filtered before being retained in the final task set. We first remove malformed records and trajectories whose geometric length falls below the minimum threshold. We then reject exact duplicates using stored trajectory signatures, ensuring that previously accepted data are not regenerated as identical samples.

To suppress near-duplicates, each remaining candidate is compared against both prior accepted trajectories and trajectories already kept in the current generation pass. Candidates are only considered comparable when their start and goal locations are within fixed spatial thresholds; for such cases, the discrete Fréchet distance is computed on resampled trajectories. A candidate is rejected if this distance falls below the similarity threshold. This post-generation filtering step improves task diversity by reducing repeated start–goal configurations, short-horizon episodes, and geometrically redundant trajectories while preserving valid long-range navigation behavior.

Generated supervision and export format. Each accepted trajectory is packaged into a goal-based navigation task with semantic target information, reference path annotations, and downstream supervision targets. Depending on the export setting, the task may further provide action labels, waypoint or trajectory supervision, first-person observations, bird’s-eye-view context, and benchmark-compatible instruction formats.

Algorithm 2 Goal-Conditioned Reference Trajectory Generation

Require: Safe grid $\mathcal{G}_{\text{safe}}$, connected components \mathcal{C} , target set \mathcal{T} , optional coverage bias
Ensure: Generated path set \mathcal{P}

- 1: $\mathcal{P} \leftarrow \emptyset$
- 2: **for** each target $\tau \in \mathcal{T}$ **do**
- 3: $g \leftarrow \tau.\text{goal_pixel}$
- 4: $c \leftarrow \tau.\text{goal_component}$
- 5: **if** zone statistics exist **then**
- 6: Sample start pixel s from component c using inverse-density zone weighting
- 7: **else if** coverage bias points exist **then**
- 8: Sample start pixel s from component c to maximize distance from prior sampled points
- 9: **else**
- 10: Uniformly sample start pixel s from component c
- 11: **end if**
- 12: $p \leftarrow \text{ASTAR}(\mathcal{G}_{\text{safe}}, s, g)$
- 13: **if** p is invalid **then continue**
- 14: **end if**
- 15: Smooth p using line-of-sight simplification
- 16: Densify the smoothed path using rasterized line segments
- 17: Adaptively resample keypoints along the path
- 18: Convert start, goal, raster path, and keypoints from pixel space to world space
- 19: Estimate start-facing direction from the first path segment
- 20: Emit one path record with semantic target, start, goal, keypoints, raster path, and metadata
- 21: $\mathcal{P} \leftarrow \mathcal{P} \cup \{p\}$
- 22: **end for**
- 23: **return** \mathcal{P}

This packaging design allows the same underlying goal-based navigation task to support multiple downstream training and evaluation settings, including both native NavGMatrix supervision and converted benchmark formats.

A.3.2 Human-Following Task Generation

We construct human-following episodes by reusing feasible goal-navigation paths and converting them into time-parameterized human motion. For each feasible path, we sample a motion category (e.g., cruise, turn, stop-and-go), retime the path with bounded speed and turn rate, and instantiate an animated human avatar along this trajectory. The agent is initialized behind the human with a preferred offset and is required to track a moving reference pose while preserving distance and viewpoint constraints.

Let the human state be $x_h^t = (p_h^t, \psi_h^t)$ and agent state be $x_a^t = (p_a^t, \psi_a^t)$ at time t . The preferred follow pose is

$$p_{\text{ref}}^t = p_h^t - d_{\text{pref}} \hat{f}_h^t + \ell \hat{r}_h^t, \quad \psi_{\text{ref}}^t = \text{atan2}(p_h^t - p_a^t),$$

where $d_{\text{pref}} \in [d_{\text{min}}, d_{\text{max}}]$ is the follow distance and $\ell \in [-\ell_{\text{max}}, \ell_{\text{max}}]$ is the lateral offset.

A.4 Instruction Generation and Benchmark Adaptation Details

To support compatibility with multiple embodied navigation benchmarks, we adapt NavGMatrix tasks into benchmark-specific instruction and action-space formats. This conversion preserves the original spatial and semantic structure of the generated tasks while making them usable in existing training and evaluation pipelines.

Instruction adaptation. Task specifications are reformulated into benchmark-compatible instruction styles aligned with VLN-CE, VLN-PE, and NaVid. Depending on the benchmark, this may involve converting semantic targets and reference trajectories into instruction-oriented task descriptions while preserving the original navigation objective.

Algorithm 3 Post-Generation Validity and Diversity Filtering

Require: Generated path set \mathcal{P} , existing accepted paths \mathcal{P}_{old}

Ensure: Filtered path set $\mathcal{P}_{\text{keep}}$

```
1: Load all prior accepted paths and their signatures
2:  $\mathcal{P}_{\text{keep}} \leftarrow \emptyset$ 
3: for each candidate path  $p \in \mathcal{P}$  do
4:   Parse path record and compute path length
5:   if  $p$  is unreadable then continue
6:   end if
7:   if path length is below minimum threshold then continue
8:   end if
9:   if signature of  $p$  already exists then continue
10:  end if
11:  similar  $\leftarrow$  False
12:  for each prior path  $q \in \mathcal{P}_{\text{old}} \cup \mathcal{P}_{\text{keep}}$  do
13:    if start distance between  $p$  and  $q$  exceeds threshold then continue
14:    end if
15:    if goal distance between  $p$  and  $q$  exceeds threshold then continue
16:    end if
17:    Compute discrete Fréchet distance between resampled versions of  $p$  and  $q$ 
18:    if distance is below similarity threshold then
19:      similar  $\leftarrow$  True
20:      break
21:    end if
22:  end for
23:  if similar then continue
24:  end if
25:  Accept  $p$ 
26:   $\mathcal{P}_{\text{keep}} \leftarrow \mathcal{P}_{\text{keep}} \cup \{p\}$ 
27: end for
28: return  $\mathcal{P}_{\text{keep}}$ 
```

Discrete action-space adaptation. In addition to instruction adaptation, the generated reference trajectories are converted into benchmark-compatible discrete action sequences. This allows NavGMATRIX to support policy-learning settings that operate on discrete control spaces rather than continuous trajectory representations.

Path generation: moving instruction. For path generation, we use a prompt that converts structured segment summaries into concise movement instructions:

System prompt:

```
You are a robotics navigation instructor. Based on the path summary, craft a concise English instruction. Describe straight segments using 'go straight for <distance> meters' without referencing heading angles. When the summary indicates a significant turn, include an explicit 'turn left' or 'turn right'. Avoid words like 'slightly'.
```

User prompt:

```
Scene: <scene_id>
Target object: <label_name>
Path summary (follow in order):
<segment_summary_lines>
Return JSON exactly as {"moving_instruction": "..."}.
```

Algorithm 4 Compact Human-Following Episode Generation

Require: Feasible nav paths \mathcal{P}_{nav} , map \mathcal{M} , params Θ

Ensure: Valid follow set \mathcal{E}

```
1:  $\mathcal{E} \leftarrow \emptyset$ 
2: for  $P \in \mathcal{P}_{\text{nav}}$  do
3:    $c \sim p(c)$ ;  $X_h \leftarrow \text{RETIMEPATH}(P, c, \Theta)$ 
4:   if  $\text{INVALIDHUMANPATH}(X_h, \mathcal{M})$  then continue
5:   end if
6:    $(d_{\text{pref}}, \ell) \leftarrow \text{SAMPLEOFFSETS}(\Theta)$ 
7:    $x_a^0 \leftarrow \text{SPAWNBEHIND}(x_h^0, d_{\text{pref}}, \ell, \mathcal{M})$ 
8:   if spawn invalid then continue
9:   end if
10:  violations  $\leftarrow 0$ 
11:  for  $t = 1, \dots, T$  do
12:     $x_{\text{ref}}^t \leftarrow \text{FOLLOWREF}(x_h^t, d_{\text{pref}}, \ell)$ 
13:     $x_a^t \leftarrow \text{TRACKERSTEP}(x_a^{t-1}, x_{\text{ref}}^t, \mathcal{M}, \Theta)$ 
14:    violations  $+= \text{CHECK}(x_a^t, x_h^t, \Theta)$ 
15:  end for
16:  if  $\text{REJECT}(\text{violations}, \Theta)$  then continue
17:  end if
18:   $\mathcal{E} \leftarrow \mathcal{E} \cup \{(X_h, X_a, c)\}$ 
19: end for
20: return  $\mathcal{E}$ 
```

Base instruction minimal grammar fix. For concise base instructions, we apply a lightweight editing prompt that performs minimal grammar correction without changing the navigation semantics:

System prompt:

You are an editor. Given a navigation instruction, make the smallest possible grammar fix to correct articles/fluency (e.g., 'an other' -> 'another', 'get a water' -> 'get some water'). Do not add extra context or change the meaning. If it is already fine, return it unchanged. Return JSON exactly as {"instruction": "..."}.

User prompt:

Scene: <scene_id>
Target object/place: <label_name>
Instruction: <instruction_text>

Detailed and benchmark-style instruction generation. For more detailed route descriptions, we generate fluent instructions from structured step breakdowns. This prompt also serves as the basis for benchmark-style instruction generation when route descriptions must be aligned with object- or landmark-aware annotation conventions:

System:

You are good at guiding the way. Generate fluent, step-by-step navigation instructions from structured inputs.

Rules:

- Keep the action order exactly as provided; never add or reorder steps.
- Select one best scene tag or landmark per step. For move/advance actions, prefer areas/rooms; for turns, prefer specific objects near the turn.
- Use natural, concise English with smooth transitions (then, next,

- after that) and no explicit numbering or the word "step".
- Do not mention distances or coordinates.
 - Mention the target only once, at the end, as the arrival point.

Style hints:

- Forward-facing point of view; describe turns as left/right relative to facing direction.
- Reference distinctive objects rather than structural elements (walls, ceilings) unless nothing else is available.
- Keep to one or two sentences total, covering all moves and turns.

Template:

{style_text}

Scene: {scene_id}

Goal object: {goal_label}

Step breakdown:

{step_breakdown}

Write the grounded instruction now.

Grounded instruction review and refinement. To improve faithfulness and linguistic quality, we further refine the generated landmark-aware instruction with a review prompt:

You are editing a navigation instruction. Keep the step order and count identical; do not add steps or landmarks that are not provided. Use at most <max_landmarks> distinct landmarks in total; avoid repeating the same landmark unless necessary. Prefer larger, distinctive landmarks; avoid ceiling/floor or tiny clutter. If landmarks are weak, keep the instruction brief. Output a single concise paragraph (no numbering or bullet points). Do not mention unavailable objects.

Goal object: <goal_label>

Step breakdown:

<step_breakdown_lines>

Available landmarks (deduped): <comma_separated_landmarks_or_none>

Raw instruction to refine:

<raw_instruction>

Rewrite now. Respond with the instruction only.

Instruction style taxonomy. We use three instruction styles in NavGMatrix:

- **Base instruction.** A short and simple target-oriented instruction used as the most concise natural-language form.
- **Detailed instruction.** A more descriptive instruction generated from structured step breakdowns and action sequences.
- **Benchmark-style instruction.** A landmark-aware instruction aligned with conventions such as VLN-CE and VLN-PE, where the route is described with reference items or scene landmarks.

Table 8 Action distribution used for dataset balancing. The balanced dataset increases the relative proportion of turning actions while preserving a smaller but meaningful proportion of stop actions.

Action	Percentage W/ Adjustment	Percentage W/O Adjustment
Forward	67%	85.6%
Turn left	15%	6.9%
Turn right	15%	6.7%
Stop	3%	0.8%
Total	100%	100%

A.5 Expanded Dataset Statistics and Balancing Details

In this section, we report expanded statistics for NavGMatrix, including task composition, path distributions, and action balancing.

Path and task statistics. We summarize additional statistics such as path length distributions, per-scene episode counts, static versus dynamic task proportions, and object-category frequency.

Action balancing. Since the raw generated dataset is strongly skewed toward forward actions, we rebalance the action distribution to improve downstream policy learning. We report the action distribution before and after balancing in the appendix.

A.6 Additional Qualitative Examples

We include additional qualitative examples to illustrate the diversity and difficulty of the generated data beyond the examples shown in the main paper.

- Additional examples of goal-based navigation trajectories.
- Additional examples of human-following episodes.
- Examples under different visual conditions.
- Challenging scenes, failure cases, and edge cases.

A.7 Model Details

A.7.1 VLM prompts

We provide the raw prompt texts used in our VLM pipeline below. The planning task uses three prompt variants, while the following task uses two variants. In implementation, the following task is instantiated as TRACKING.

Planning prompt with RGB, history, BEV, and OCC.

<image><image><image><image>

You are given FOUR images from the same navigation episode.

Image 1: CURRENT first-person RGB.

Image 2: HISTORY mosaic (4x4), NEW->OLD sampled by discrete action steps (current excluded; missing => black).

Image 3: Scene-level BEV map.

Image 4: OCC / traversability map (ORIGINAL resolution). Green=start, Red=current, white=traversable.

TASK_TYPE: PLANNING

Instruction: "{INSTRUCTION_TEXT}"

COORDS (Image 4, normalized tokens):

- Each coordinate is ($\langle x_norm \rangle, \langle y_norm \rangle$) as tokens $\langle 0 \rangle .. \langle 999 \rangle$.
- OCC size: $W = \{OCC_W\}$ px, $H = \{OCC_H\}$ px
- Normalize: $x_norm = \text{round_half_up}(x_px / W * 1000)$, $y_norm = \text{round_half_up}(y_px / H * 1000)$, clip $[0, 999]$.
- Scale: 1 $x_norm = \{X_NORM_UNIT_M\}$ m, 1 $y_norm = \{Y_NORM_UNIT_M\}$ m. (1 px = $\{OCC_M_PER_PX\}$ m)

CURRENT_PIXEL (normalized): ($\{CUR_XN\}, \{CUR_YN\}$)

Your task (return all branches aligned):

- (A) Waypoints on Image 4, normalized tokens, 13 points: current + 12 future.
- Point0 = CURRENT_PIXEL.
 - Points1..12 follow future path with 0.25m spacing (3.0m total); pad with last if short.
- (B) Actions: exactly 6 tokens from $\{\langle FWD \rangle, \langle LEFT \rangle, \langle RIGHT \rangle, \langle STOP \rangle\}$ matching (A).
- Action semantics: $\langle FWD \rangle$ moves forward 0.25m; $\langle LEFT \rangle / \langle RIGHT \rangle$ rotate 15 degrees in place (no translation); $\langle STOP \rangle$ means stop.

Output (STRICT): JSON with keys "pixel" and "vlnce".

- "pixel": "[[$\langle x0 \rangle, \langle y0 \rangle$],..., (13 pts)]"
 - "vlnce": " $\langle action \rangle \langle FWD \rangle, \dots, \langle STOP \rangle \langle /action \rangle$ "
- No extra text.

Planning prompt with BEV and OCC.

$\langle image \rangle \langle image \rangle$

You are given TWO images from the same navigation episode.

Image 1: Scene-level BEV map.

Image 2: OCC / traversability map (ORIGINAL resolution). Green=start, Red=current, white=traversable.

TASK_TYPE: PLANNING

Instruction: "{INSTRUCTION_TEXT}"

COORDS (Image 2, normalized tokens):

- Each coordinate is ($\langle x_norm \rangle, \langle y_norm \rangle$) as tokens $\langle 0 \rangle .. \langle 999 \rangle$.
- OCC size: $W = \{OCC_W\}$ px, $H = \{OCC_H\}$ px
- Normalize: $x_norm = \text{round_half_up}(x_px / W * 1000)$, $y_norm = \text{round_half_up}(y_px / H * 1000)$, clip $[0, 999]$.
- Scale: 1 $x_norm = \{X_NORM_UNIT_M\}$ m, 1 $y_norm = \{Y_NORM_UNIT_M\}$ m. (1 px = $\{OCC_M_PER_PX\}$ m)

CURRENT_PIXEL (normalized): ($\{CUR_XN\}, \{CUR_YN\}$)

Your task (return all branches aligned):

- (A) Waypoints on Image 2, normalized tokens, 13 points: current + 12 future.
- Point0 = CURRENT_PIXEL.
 - Points1..12 follow future path with 0.25m spacing (3.0m total); pad with last if short.
- (B) Actions: exactly 6 tokens from $\{\langle FWD \rangle, \langle LEFT \rangle, \langle RIGHT \rangle, \langle STOP \rangle\}$ matching (A).
- Action semantics: $\langle FWD \rangle$ moves forward 0.25m; $\langle LEFT \rangle / \langle RIGHT \rangle$ rotate 15 degrees in place (no translation); $\langle STOP \rangle$ means stop.

Output (STRICT): JSON with keys "pixel" and "vlnce".

- "pixel": "[[$\langle x0 \rangle, \langle y0 \rangle$],..., (13 pts)]"
 - "vlnce": " $\langle action \rangle \langle FWD \rangle, \dots, \langle STOP \rangle \langle /action \rangle$ "
- No extra text.

Planning prompt with RGB and history only.

$\langle image \rangle \langle image \rangle$

You are given TWO images from the same navigation episode.

Image 1: CURRENT first-person RGB.

Image 2: HISTORY mosaic (4x4), NEW->OLD sampled by discrete action steps (current excluded; missing => black).

TASK_TYPE: PLANNING

Instruction: "{INSTRUCTION_TEXT}"

Your task:

- Actions: exactly 6 tokens from {{<FWD>,<LEFT>,<RIGHT>,<STOP>}}.
- Action semantics: <FWD> moves forward 0.25m; <LEFT>/ <RIGHT> rotate 15 degrees in place (no translation); <STOP> means stop.

Output (STRICT): JSON with key "vlnce".

- "vlnce": "<action><FWD>,...,<STOP></action>"

No extra text.

Following prompt with FPV, BEV, and OCC.

<image><image><image><image>

You are given FOUR images from the same navigation episode.

Image 1: CURRENT first-person RGB.

Image 2: HISTORY mosaic (4x4), ALL BLACK for tracking.

Image 3: Scene-level BEV map.

Image 4: OCC / traversability map (ORIGINAL resolution). Green=start, Red=current, white=traversable.

TASK_TYPE: TRACKING

Instruction: "{INSTRUCTION_TEXT}"

COORDS (Image 4, normalized tokens):

- Each coordinate is (<x_norm>,<y_norm>) as tokens <0>..<999>.
- OCC size: W={OCC_W} px, H={OCC_H} px
- Normalize: $x_norm = \text{round_half_up}(x_px/W*1000)$, $y_norm = \text{round_half_up}(y_px/H*1000)$, clip [0,999].
- Scale: $1\ x_norm = \{X_NORM_UNIT_M\}\ m$, $1\ y_norm = \{Y_NORM_UNIT_M\}\ m$. (1 px = {OCC_M_PER_PX} m)

CURRENT_PIXEL (normalized): ({CUR_XN},{CUR_YN})

Your task (return both branches aligned):

- (A) Waypoints on Image 4, normalized tokens, 7 points: current + 6 future.
 - Point0 = CURRENT_PIXEL; pad with last if short.
- (B) Actions: exactly 6 tokens from {{<FWD>,<LEFT>,<RIGHT>,<STOP>}} matching (A).
 - Action semantics: <FWD> moves forward 0.25m; <LEFT>/ <RIGHT> rotate 15 degrees in place (no translation); <STOP> means stop.

Output (STRICT): JSON with keys "pixel" and "vlnce".

- "pixel": "[[<x0>,<y0>],..., (7 pts)]"

- "vlnce": "<action><FWD>,...,<STOP></action>"

No extra text.

Following prompt with FPV only.

<image><image>

You are given TWO images from the same navigation episode.

Image 1: CURRENT first-person RGB.

Image 2: HISTORY mosaic (4x4), ALL BLACK for tracking.

TASK_TYPE: TRACKING
Instruction: "{INSTRUCTION_TEXT}"

Your task:

- Actions: exactly 6 tokens from $\{\{<FWD>, <LEFT>, <RIGHT>, <STOP>\}\}$.
- Action semantics: $<FWD>$ moves forward 0.25m; $<LEFT>/ <RIGHT>$ rotate 15 degrees in place (no translation); $<STOP>$ means stop.

Output (STRICT): JSON with key "vlnce".

- "vlnce": " $<action><FWD>, \dots, <STOP></action>$ "
- No extra text.

References

- Peter Anderson, Qi Wu, Damien Teney, Jake Bruce, Mark Johnson, Niko Sünderhauf, Ian Reid, Stephen Gould, and Anton Van Den Hengel. Vision-and-language navigation: Interpreting visually-grounded navigation instructions in real environments. In *Proceedings of the IEEE Conference on Computer Vision and Pattern Recognition*, pages 3674–3683, 2018a.
- Vihan Jain, Gabriel Ilharco, Alexander Ku, Ashish Vaswani, Eugene Ie, and Jason Baldridge. Stay on the path: Instruction fidelity in vision-and-language navigation. In *Annual Meeting of the Association for Computational Linguistics*, 2019.
- Jacob Krantz, Erik Wijmans, Arjun Majumdar, Dhruv Batra, and Stefan Lee. Beyond the nav-graph: Vision-and-language navigation in continuous environments. In *European Conference on Computer Vision*, pages 104–120. Springer, 2020.
- Bernhard Kerbl, Georgios Kopanas, Thomas Leimkühler, and George Drettakis. 3d gaussian splatting for real-time radiance field rendering. *ACM Transactions on Graphics*, 42(4), July 2023.
- Binbin Huang, Zehao Yu, Anpei Chen, Andreas Geiger, and Shenghua Gao. 2d gaussian splatting for geometrically accurate radiance fields. In *ACM SIGGRAPH 2024 conference papers*, pages 1–11, 2024.
- Danpeng Chen, Hai Li, Weicai Ye, Yifan Wang, Weijian Xie, Shangjin Zhai, Nan Wang, Haomin Liu, Hujun Bao, and Guofeng Zhang. Pgsr: Planar-based gaussian splatting for efficient and high-fidelity surface reconstruction. *IEEE Transactions on Visualization and Computer Graphics*, 31(9):6100–6111, 2024a.
- Ben Poole, Ajay Jain, Jonathan T Barron, and Ben Mildenhall. Dreamfusion: Text-to-3d using 2d diffusion. *arXiv preprint arXiv:2209.14988*, 2022.
- Xinhai Li, Huaibin Wang, and Kuo-Kun Tseng. Gaussiandiffusion: 3d gaussian splatting for denoising diffusion probabilistic models with structured noise. *arXiv preprint arXiv:2311.11221*, 2023.
- Zibo Zhao, Zeqiang Lai, Qingxiang Lin, Yunfei Zhao, Haolin Liu, Shuhui Yang, Yifei Feng, Mingxin Yang, Sheng Zhang, Xianghui Yang, et al. Hunyuan3d 2.0: Scaling diffusion models for high resolution textured 3d assets generation. *arXiv preprint arXiv:2501.12202*, 2025.
- Jianfeng Xiang, Zelong Lv, Sicheng Xu, Yu Deng, Ruicheng Wang, Bowen Zhang, Dong Chen, Xin Tong, and Jiaolong Yang. Structured 3d latents for scalable and versatile 3d generation. In *Proceedings of the IEEE/CVF conference on computer vision and pattern recognition*, pages 21469–21480, 2025.
- Haozhe Lou, Yurong Liu, Yike Pan, Yiran Geng, Jianteng Chen, Wenlong Ma, Chenglong Li, Lin Wang, Hengzhen Feng, Lu Shi, et al. Robo-gs: A physics consistent spatial-temporal model for robotic arm with hybrid representation. In *2025 IEEE International Conference on Robotics and Automation (ICRA)*, pages 15379–15386. IEEE, 2025.
- Xinhai Li, Jialin Li, Ziheng Zhang, Rui Zhang, Fan Jia, Tiancai Wang, Haoqiang Fan, Kuo-Kun Tseng, and Ruiping Wang. Robogsim: A real2sim2real robotic gaussian splatting simulator. *arXiv preprint arXiv:2411.11839*, 2024.
- M Nomaan Qureshi, Sparsh Garg, Francisco Yandun, David Held, George Kantor, and Abhisesh Silwal. Splatsim: Zero-shot sim2real transfer of rgb manipulation policies using gaussian splatting. In *2025 IEEE International Conference on Robotics and Automation (ICRA)*, pages 6502–6509. IEEE, 2025.
- Liuyi Wang, Xinyuan Xia, Hui Zhao, Hanqing Wang, Tai Wang, Yilun Chen, Chengju Liu, Qijun Chen, and Jiangmiao Pang. Rethinking the embodied gap in vision-and-language navigation: A holistic study of physical and visual disparities. *arXiv preprint arXiv:2507.13019*, 2025a.

- Xiaohan Lei, Min Wang, Wengang Zhou, and Houqiang Li. Gaussnav: Gaussian splatting for visual navigation. IEEE Transactions on Pattern Analysis and Machine Intelligence, 47(5):4108–4121, 2025.
- Bingchen Miao, Rong Wei, Zhiqi Ge, Xiaoquan Sun, Shiqi Gao, Jingzhe Zhu, Renhan Wang, Siliang Tang, Jun Xiao, Rui Tang, and Juncheng Li. Towards physically executable 3d gaussian for embodied navigation. In The Fourteenth International Conference on Learning Representations, 2026.
- Sikuang Li, Chen Yang, Jiemin Fang, Taoran Yi, Jia Lu, Jiazhong Cen, Lingxi Xie, Wei Shen, and Qi Tian. Worldgrow: Generating infinite 3d world. arXiv preprint arXiv:2510.21682, 2025.
- Johannes Lutz Schönberger, True Price, Torsten Sattler, Jan-Michael Frahm, and Marc Pollefeys. A vote-and-verify strategy for fast spatial verification in image retrieval. In Asian Conference on Computer Vision (ACCV), 2016.
- Yifei Dong, Fengyi Wu, Qi He, Heng Li, Minghan Li, Zebang Cheng, Yuxuan Zhou, Jingdong Sun, Qi Dai, Zhi-Qi Cheng, et al. Ha-vln: A benchmark for human-aware navigation in discrete-continuous environments with dynamic multi-human interactions, real-world validation, and an open leaderboard. arXiv preprint, 2025.
- Jonah Philion and Sanja Fidler. Lift, splat, shoot: Encoding images from arbitrary camera rigs by implicitly unprojecting to 3d. In European Conference on Computer Vision, pages 194–210. Springer, 2020.
- Chenyu Yang, Yuntao Chen, Hao Tian, Chenxin Tao, Xizhou Zhu, Zhaoxiang Zhang, Gao Huang, Hongyang Li, Yu Qiao, Lewei Lu, et al. Bevformer v2: Adapting modern image backbones to bird’s-eye-view recognition via perspective supervision. In Proceedings of the IEEE/CVF Conference on Computer Vision and Pattern Recognition, pages 17830–17839, 2023.
- Jiaqi Chen, Bingqian Lin, Ran Xu, Zhenhua Chai, Xiaodan Liang, and Kwan-Yee K. Wong. Mapgpt: Map-guided prompting with adaptive path planning for vision-and-language navigation. In Proceedings of the 62nd Annual Meeting of the Association for Computational Linguistics, 2024b.
- Wenzhe Cai, Jiaqi Peng, Yuqiang Yang, Yujian Zhang, Meng Wei, Hanqing Wang, Yilun Chen, Tai Wang, and Jiangmiao Pang. Navdp: Learning sim-to-real navigation diffusion policy with privileged information guidance. arXiv preprint arXiv:2505.08712, 2025.
- Shuai Bai, Yuxuan Cai, Ruizhe Chen, Keqin Chen, Xionghui Chen, Zesen Cheng, Lianghao Deng, Wei Ding, Chang Gao, Chunjiang Ge, Wenbin Ge, Zhifang Guo, Qidong Huang, Jie Huang, Fei Huang, Binyuan Hui, Shutong Jiang, Zhaohai Li, Mingsheng Li, Mei Li, Kaixin Li, Zicheng Lin, Junyang Lin, Xuejing Liu, Jiawei Liu, Chenglong Liu, Yang Liu, Dayiheng Liu, Shixuan Liu, Dunjie Lu, Ruilin Luo, Chenxu Lv, Rui Men, Lingchen Meng, Xuancheng Ren, Xingzhang Ren, Sibao Song, Yuchong Sun, Jun Tang, Jianhong Tu, Jianqiang Wan, Peng Wang, Pengfei Wang, Qiuyue Wang, Yuxuan Wang, Tianbao Xie, Yiheng Xu, Haiyang Xu, Jin Xu, Zhibo Yang, Mingkun Yang, Jianxin Yang, An Yang, Bowen Yu, Fei Zhang, Hang Zhang, Xi Zhang, Bo Zheng, Humen Zhong, Jingren Zhou, Fan Zhou, Jing Zhou, Yuanzhi Zhu, and Ke Zhu. Qwen3-vl technical report. arXiv preprint arXiv:2511.21631, 2025.
- Zhihong Shao, Peiyi Wang, Qihao Zhu, Runxin Xu, Junxiao Song, Xiao Bi, Haowei Zhang, Mingchuan Zhang, Y. K. Li, Y. Wu, and Daya Guo. Deepseekmath: Pushing the limits of mathematical reasoning in open language models, 2024.
- Shaoan Wang, Jiazhao Zhang, Minghan Li, Jiahang Liu, Anqi Li, Kui Wu, Fangwei Zhong, Junzhi Yu, Zhizheng Zhang, and He Wang. Trackvla: Embodied visual tracking in the wild. arXiv preprint arXiv:2505.23189, 2025b.
- Yihan Cao, Jiazhao Zhang, Zhinan Yu, Shuzhen Liu, Zheng Qin, Qin Zou, Bo Du, and Kai Xu. Cognav: Cognitive process modeling for object goal navigation with llms. In Proceedings of the IEEE/CVF International Conference on Computer Vision, pages 9550–9560, 2025.
- Chen Gao, Liankai Jin, Xingyu Peng, Jiazhao Zhang, Yue Deng, Annan Li, He Wang, and Si Liu. Octonav: Towards generalist embodied navigation. arXiv preprint arXiv:2506.09839, 2025.
- Jiahang Liu, Yunpeng Qi, Jiazhao Zhang, Minghan Li, Shaoan Wang, Kui Wu, Hanjing Ye, Hong Zhang, Zhibo Chen, Fangwei Zhong, et al. Trackvla++: Unleashing reasoning and memory capabilities in vla models for embodied visual tracking. arXiv preprint arXiv:2510.07134, 2025.
- Sunyao Zhou, Yunzi Wu, Tianhang Wang, Xinhai Li, Guang Chen, Lizheng Liu, Chenjia Bai, and Xuelong Li. Deconav: Dialog enhanced long-horizon collaborative vision-language navigation. arXiv preprint arXiv:2604.12486, 2026.
- Hongjun An, Wenhan Hu, Sida Huang, Siqi Huang, Ruanjun Li, Yuanzhi Liang, Jiawei Shao, Yiliang Song, Zihan Wang, Cheng Yuan, et al. Ai flow: Perspectives, scenarios, and approaches. Vicinagearth, 3(1):1, 2026.

- Shizhe Chen, Pierre-Louis Guhur, Makarand Tapaswi, Cordelia Schmid, and Ivan Laptev. Think global, act local: Dual-scale graph transformer for vision-and-language navigation. 2022 IEEE/CVF Conference on Computer Vision and Pattern Recognition (CVPR), pages 16516–16526, 2022a.
- Gengze Zhou, Yicong Hong, and Qi Wu. Navgpt: Explicit reasoning in vision-and-language navigation with large language models. In AAAI Conference on Artificial Intelligence, 2023.
- Tianyu Xu, Jiawei Chen, Jiazhao Zhang, Wenyao Zhang, Zekun Qi, Minghan Li, Zhizheng Zhang, and He Wang. Mm-nav: Multi-view vla model for robust visual navigation via multi-expert learning. arXiv preprint arXiv:2510.03142, 2025.
- Duo Zheng, Shijia Huang, Lin Zhao, Yiwu Zhong, and Liwei Wang. Towards learning a generalist model for embodied navigation. In Proceedings of the IEEE/CVF Conference on Computer Vision and Pattern Recognition, pages 13624–13634, 2024.
- Yuehao Huang, Liang Liu, Shuangming Lei, Yukai Ma, Hao Su, Jianbiao Mei, Pengxiang Zhao, Yaqing Gu, Yong Liu, and Jiajun Lv. Cogddn: A cognitive demand-driven navigation with decision optimization and dual-process thinking. In Proceedings of the 33rd ACM International Conference on Multimedia, pages 5237–5246, 2025.
- InternNav Team. InternVLA-N1: An open dual-system navigation foundation model with learned latent plans, 2025.
- Zedong Chu, Shichao Xie, Xiaolong Wu, Yanfen Shen, Minghua Luo, Zhengbo Wang, Fei Liu, Xiaoxu Leng, Junjun Hu, Mingyang Yin, Jia Lu, Yingnan Guo, Kai Yang, Jiawei Han, Xu Chen, Yanqing Zhu, Yuxiang Zhao, Xin Liu, Yirong Yang, Ye He, Jiahang Wang, Yang Cai, Tianlin Zhang, Li Gao, Liu Liu, Mingchao Sun, Fan Jiang, Chiyu Wang, Zhicheng Liu, Hongyu Pan, Honglin Han, Zhining Gu, Kuan Yang, Jianfang Zhang, Di Jing, Zihao Guan, Wei Guo, Guoqing Liu, Di Yang, Xiangpo Yang, Menglin Yang, Hongguang Xing, Weiguang Li, and Mu Xu. Abot-n0: Technical report on the vla foundation model for versatile embodied navigation, 2026.
- Dong An, Hanqing Wang, Wenguan Wang, Zun Wang, Yan Huang, Keji He, and Liang Wang. Etpnav: Evolving topological planning for vision-language navigation in continuous environments. IEEE Transactions on Pattern Analysis and Machine Intelligence, 2024.
- Thomas Chabal, Shizhe Chen, Jean Ponce, and Cordelia Schmid. Fom-nav: Frontier-object maps for object goal navigation, 2025. URL <https://arxiv.org/abs/2512.01009>.
- Yuncong Yang, Han Yang, Jiachen Zhou, Peihao Chen, Hongxin Zhang, Yilun Du, and Chuang Gan. 3d-mem: 3d scene memory for embodied exploration and reasoning. In Proceedings of the IEEE/CVF Conference on Computer Vision and Pattern Recognition, pages 17294–17303, 2025.
- Jiazhao Zhang, Kunyu Wang, Shaoan Wang, Minghan Li, Haoran Liu, Songlin Wei, Zhongyuan Wang, Zhizheng Zhang, and He Wang. Uni-navid: A video-based vision-language-action model for unifying embodied navigation tasks. Robotics: Science and Systems, 2025.
- Ziyi Chen, Yingnan Guo, Zedong Chu, Minghua Luo, Yanfen Shen, Mingchao Sun, Junjun Hu, Shichao Xie, Kuan Yang, Pei Shi, Zhining Gu, Lu Liu, Honglin Han, Xiaolong Wu, Mu Xu, Yu Zhang, and Ning Guo. Socialnav: Training human-inspired foundation model for socially-aware embodied navigation, 2026.
- Manycore Tech Inc. SpatialVerse Research Team. InteriorGS: A 3d gaussian splatting dataset of semantically labeled indoor scenes. <https://huggingface.co/datasets/spatialverse/InteriorGS>, 2025.
- Xinshuai Song, Weixing Chen, Yang Liu, Weikai Chen, Guanbin Li, and Liang Lin. Towards long-horizon vision-language navigation: Platform, benchmark and method. In Proceedings of the IEEE/CVF Conference on Computer Vision and Pattern Recognition, pages 12078–12088, 2025.
- Tianhang Wang, Xinhai Li, Fan Lu, Tianshi Gong, Jiankun Dong, Weiyi Xue, Sanqing Qu, Chenjia Bai, and Guang Chen. Conavbench: Collaborative long-horizon vision-language navigation benchmark. In The Fourteenth International Conference on Learning Representations, 2026.
- Zhi Jing, Jinbin Qiao, Ouyang Lu, Jicong Ao, Shuang Qiu, Yu-Gang Jiang, and Chenjia Bai. Assemblm: Spatial reasoning multimodal large language models for robotic assembly. arXiv preprint arXiv:2604.08983, 2026.
- Jiazhao Zhang, Kunyu Wang, Rongtao Xu, Gengze Zhou, Yicong Hong, Xiaomeng Fang, Qi Wu, Zhizheng Zhang, and He Wang. Navid: Video-based vlm plans the next step for vision-and-language navigation. Robotics: Science and Systems, 2024.

- Mukul Khanna*, Yongsan Mao*, Hanxiao Jiang, Sanjay Haresh, Brennan Shacklett, Dhruv Batra, Alexander Clegg, Eric Undersander, Angel X. Chang, and Manolis Savva. Habitat Synthetic Scenes Dataset (HSSD-200): An Analysis of 3D Scene Scale and Realism Tradeoffs for ObjectGoal Navigation. arXiv preprint, 2023.
- Peter E. Hart, Nils J. Nilsson, and Bertram Raphael. A formal basis for the heuristic determination of minimum cost paths. IEEE Transactions on Systems Science and Cybernetics, 4(2):100–107, 1968.
- J. Richalet, A. Rault, J. L. Testud, and J. Papon. Model predictive heuristic control: Applications to industrial processes. Automatica, 14(5):413–428, 1978.
- Manolis Savva, Abhishek Kadian, Oleksandr Maksymets, Yili Zhao, Erik Wijmans, Bhavana Jain, Julian Straub, Jia Liu, Vladlen Koltun, Jitendra Malik, et al. Habitat: A platform for embodied ai research. In Proceedings of the IEEE/CVF International Conference on Computer Vision, pages 9339–9347, 2019.
- Jiahang Liu, Yuanxing Duan, Jiazhao Zhang, Minghan Li, Shaoan Wang, Zhizheng Zhang, and He Wang. Navgsim: High-fidelity gaussian splatting simulator for large-scale navigation, 2026.
- J. E. Bresenham. Algorithm for computer control of a digital plotter. IBM Systems Journal, 4(1):25–30, 1965. doi: 10.1147/sj.41.0025.
- Peter Anderson, Angel Chang, Devendra Singh Chaplot, Alexey Dosovitskiy, Saurabh Gupta, Vladlen Koltun, Jana Kosecka, Jitendra Malik, Roozbeh Mottaghi, Manolis Savva, et al. On evaluation of embodied navigation agents. arXiv preprint arXiv:1807.06757, 2018b.
- Stéphane Ross, Geoffrey Gordon, and Drew Bagnell. A reduction of imitation learning and structured prediction to no-regret online learning. In Proceedings of the fourteenth international conference on artificial intelligence and statistics, pages 627–635. JMLR Workshop and Conference Proceedings, 2011.
- Qiyang Yu, Zheng Zhang, Ruofei Zhu, Yufeng Yuan, Xiaochen Zuo, Yu Yue, Weinan Dai, Tiantian Fan, Gaohong Liu, Lingjun Liu, Xin Liu, Haibin Lin, Zhiqi Lin, Bole Ma, Guangming Sheng, Yuxuan Tong, Chi Zhang, Mofan Zhang, Wang Zhang, Hang Zhu, Jinhua Zhu, Jiaye Chen, Jiangjie Chen, Chengyi Wang, Hongli Yu, Yuxuan Song, Xiangpeng Wei, Hao Zhou, Jingjing Liu, Wei-Ying Ma, Ya-Qin Zhang, Lin Yan, Mu Qiao, Yonghui Wu, and Mingxuan Wang. Dapo: An open-source llm reinforcement learning system at scale, 2025.
- Ting Chen, Saurabh Saxena, Lala Li, David J. Fleet, and Geoffrey Hinton. Pix2seq: A language modeling framework for object detection. In International Conference on Learning Representations, 2022b.
- Ting Chen, Saurabh Saxena, Lala Li, Tsung-Yi Lin, David J. Fleet, and Geoffrey Hinton. A unified sequence interface for vision tasks. In Advances in Neural Information Processing Systems, 2022c.
- Zhiliang Peng, Wenhui Wang, Li Dong, Yaru Hao, Shaohan Huang, Shuming Ma, Qixiang Ye, and Furu Wei. Kosmos-2: Grounding multimodal large language models to the world. In International Conference on Learning Representations, 2024.
- Qing Jiang, Junan Huo, Xingyu Chen, Yuda Xiong, Zhaoyang Zeng, Yihao Chen, Tianhe Ren, Junzhi Yu, and Lei Zhang. Detect anything via next point prediction, 2025.
- John Schulman, Filip Wolski, Prafulla Dhariwal, Alec Radford, and Oleg Klimov. Proximal policy optimization algorithms, 2017.
- Jonathan Ho, Ajay Jain, and Pieter Abbeel. Denoising diffusion probabilistic models. In Advances in Neural Information Processing Systems, volume 33, pages 6840–6851, 2020.
- Cheng Chi, Zhenjia Xu, Siyuan Feng, Eric Cousineau, Yilun Du, Benjamin Burchfiel, Russ Tedrake, and Shuran Song. Diffusion policy: Visuomotor policy learning via action diffusion. In Robotics: Science and Systems, 2023.